

0-A128 452

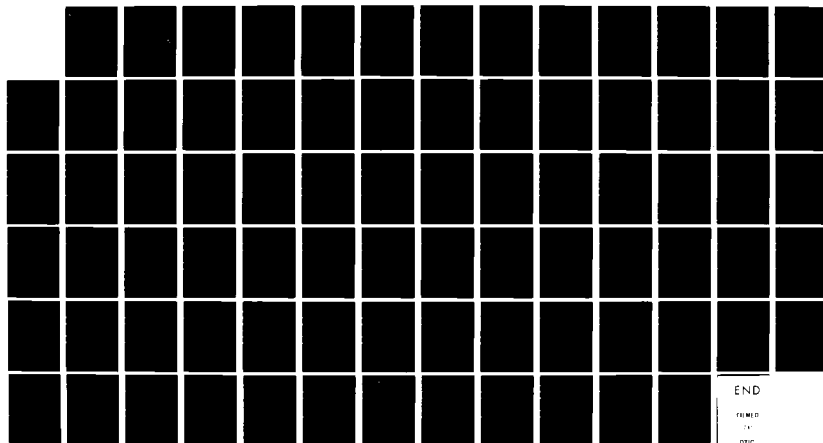
STUDY OF BOUNDARY STRUCTURES(U) HUGHES RESEARCH LABS  
MALIBU CA R KIKUCHI SEP 82 ARO-16468.2-PH  
DRAG29-79-C-0898

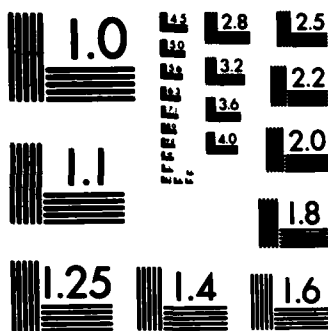
1/1

UNCLASSIFIED

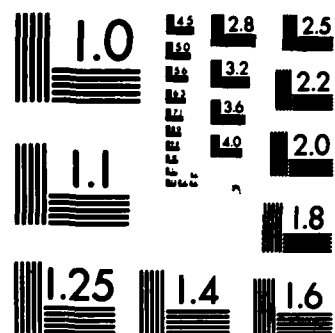
F/G 20/2

NL

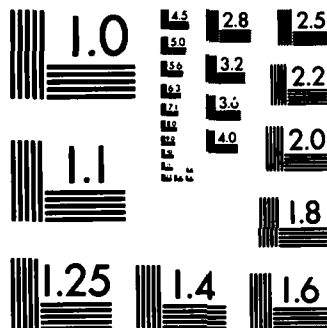




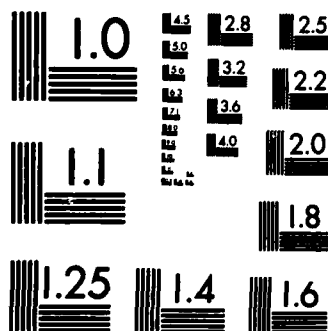
MICROCOPY RESOLUTION TEST CHART  
NATIONAL BUREAU OF STANDARDS-1963-A



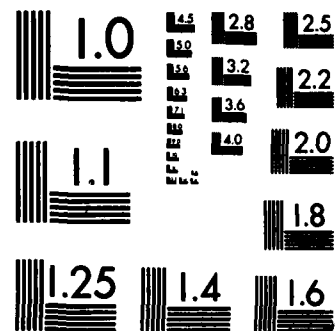
MICROCOPY RESOLUTION TEST CHART  
NATIONAL BUREAU OF STANDARDS-1963-A



MICROCOPY RESOLUTION TEST CHART  
NATIONAL BUREAU OF STANDARDS-1963-A



MICROCOPY RESOLUTION TEST CHART  
NATIONAL BUREAU OF STANDARDS-1963-A



MICROCOPY RESOLUTION TEST CHART  
NATIONAL BUREAU OF STANDARDS-1963-A

ARO 16468. 2-PH

(12)

## STUDY OF BOUNDARY STRUCTURES

R. Kikuchi

Hughes Research Laboratories  
3011 Malibu Canyon Road  
Malibu, CA 90265

September 1982

DAAG29-79-C0090

Final Report

For Period 1 May 1979 through 30 June 1982

DTIC  
OCT 19 1982  
H

U.S. ARMY RESEARCH OFFICE  
Research Triangle Park, NC 27709

DISTRIBUTION STATEMENT A  
Approved for public release;  
Distribution Unlimited

82 10 18 118

AD A120452

DTIC FILE COPY

**SECURITY CLASSIFICATION OF THIS PAGE (When Data Entered)**

DD FORM 1 JAN 73 1473 EDITION OF 1 NOV 65 IS OBSOLETE

SECURITY CLASSIFICATION OF THIS PAGE (When Data Entered)

UNCLASSIFIED

SECURITY CLASSIFICATION OF THIS PAGE (When Data Entered)

CVM. The layers on the left of the boundary are perpendicular to the layers on the right-hand side. By calculating the excess free energy and the amount of adsorbed Au atoms, a first-order phase transition is derived within the boundary; there is a discontinuous change in the Au adsorption as the overall composition of the system changes across the stoichiometric state. Also there is a switch-over from the low temperature phase to the high-temperature phase; the difference of the two phases is in the behavior of the layer parallel to the boundary.

The ABC-CBA stacking boundary in the fcc lattice in the (110) direction is also studied. A reference hexagonal lattice with three times as many lattice points as the original fcc lattice is considered by supplementing the latter by interstitial points; atoms are assumed to move on the reference hexagonal lattice. A three-layer rhombus prism of 12 lattice points is used as the basic cluster of the CVM. The equilibrium structure of the boundary is obtained by minimizing the grand potential, keeping the chemical potential fixed. The set of nonlinear simultaneous algebraic equations of 90,000 variables are solved using the Natural Iteration Method and using the CRAY computer. Thermodynamic quantities and the density profile are obtained, but the number of calculated points are still too small to conclude useful results. Further studies are planned.

UNCLASSIFIED

SECURITY CLASSIFICATION OF THIS PAGE (When Data Entered)

# TABLE OF CONTENTS

SECTION		PAGE
1	INTRODUCTION AND SUMMARY.....	7
2	FIRST ORDER TRANSITIONS WITHIN ROTATIONAL APB's IN L1 <sub>0</sub> PHASE.....	9
3	THEORY OF ABC-CBA STACKING BOUNDARY IN fcc STRUCTURE.....	11
4	TRANSITIONS AND PHASE EQUILIBRIA AMONG GRAIN BOUNDARY STRUCTURES.....	13
	ACKNOWLEDGMENT.....	15
	REFERENCES.....	17
APPENDICES		
A	FIRST ORDER TRANSITION WITHIN ROTATIONAL APB's IN L1 <sub>0</sub> PHASE.....	19
B	THEORY OF ABC-CBA STACKING BOUNDARY IN fcc STRUCTURE.....	37
C	TRANSITIONS AND PHASE EQUILIBRIA AMONG GRAIN BOUNDARY STRUCTURES.....	71



Accession For	
NTIS GRA&I	<input checked="" type="checkbox"/>
DTIC TAB	<input type="checkbox"/>
Unannounced	<input type="checkbox"/>
Justification	
By	
Distribution/	
Availability Codes	
Dist	Avail and/or Special
A	

# LIST OF ILLUSTRATIONS

FIGURE		PAGE
App. A		
1	Structure of the 90°-rotational APB.....	21
2	Density profile of Au atoms on the four sublattices across boundary at $kT/ w  = 0.7$ .....	24
3	Adsorption of Au atoms at the boundary plotted against temperature.....	27
4	Schematic diagram of $\sigma$ versus $\mu$ at a constant temperature.....	28
5	The Au density, $x(2)$ , on sublattices I and III plotted against the Au density in the bulk phase at $kT/ w  = 0.7$ .....	30
6	Density profile of Au atoms on the four sublattices across the boundary at $kT/ w  = 0.7$ and for $\mu = 1.3$ .....	31
7	The excess Au adsorbed at the surface against the overall density of Au throughout the system.....	32
8	The excess free energy $\sigma$ at the stoichiometric composition plotted against temperature.....	33
9	The chemical potential $\mu$ plotted against the density of Au in the bulk homogeneous phase.....	34
App. B		
1	The reference lattice points A, B, and C on the layer "1" of the fcc lattice.....	39
2	The ABC and CBA stackings in the fcc lattice.....	40
3	The (112) boundary corresponding to Figure 2.....	42
4	The shapes of the clusters used in the CVM treatment.....	43
5	The long-range order parameter in the homogeneous bulk phase plotted against the temperature at $\mu/\epsilon = -4.0$ .....	64
6	Density of atoms on each sublattice, at $kT/\epsilon = 4$ and $\mu/\epsilon = -4$ .....	67

FIGURE

PAGE

App. C

- 1      The same tangent constructio is used for the coexistence  
of phases, using a cartesian plot of molar free energy vs.  
composition, and of facets, using a polar plot of  $\gamma^1(N)$ .....      75
- 2      The inner envelope of a  $\xi$  plot shows the actual orientations  
of stable boundaries.....      76
- 3      Forms of  $\xi$  plots must conform to the symmetry of the Wulff  
group.....      80
- 4      Portions of an N diagram straddling a mirror plane.....      84



## SECTION 1

### INTRODUCTION AND SUMMARY

This project studies the atomic structures of boundaries. The tool used in the study is the cluster variation method (CVM) of statistical mechanics, with the work leading to information on excess free energy (surface tension), excess entropy, and the amount of adsorption and the profile of the density across the boundary. This project is unique in obtaining such information from a microscopic point of view. And while different from some phenomenological approaches, the CVM technique is thermodynamically consistent, in the sense that thermodynamic relations are always satisfied.

In the period preceding the present report time frame, we pursued three different directions. The first considered the boundaries in binary fcc crystals, the second examined the grain boundary structure, and the third was concerned with the scalar-product expression of the boundary free energy. In the present report period, the work in the first two categories has been further exploited.

(A) In working with the statistical mechanics of binary fcc alloys we need a tetrahedron made of four lattice points.<sup>1,2</sup> Our two previous papers<sup>3,4</sup> worked on the antiphase and interphase boundaries (APB and IPB) in the Cu<sub>3</sub>Au ordered phase and the disordered phase using a tetrahedron. We found that the boundary free energy,  $\sigma$  (of both APB and IPB), goes through a maximum when plotted against the temperature. This behavior of  $\sigma$  is similar to the yield strength of the material and suggests the close relation between the two properties.

The work on the fcc boundaries has been continued and a rotational APB in CuAu ordered phase has been studied, as is reported in Appendix A. Different from our previous work in Refs. 3 and 4, the left- and right-hand sides of this boundary are not symmetrical. Because of the asymmetry, the boundary behaves in a markedly different way from previous boundaries. By contrast, a first order phase transition occurs within the boundary. The amount of adsorption of Au atoms at the boundary changes sign as the temperature increases. Another kind of phase transition is also derived at a non-stoichiometric composition.

Although the theory is thermodynamically self-consistent, we decided, because these findings are so unique, to spend ample time to verify the accuracy of the theory before publishing the result.

(B) In previous studies of the structure of a two-dimensional grain boundary<sup>5</sup> we used a DSC lattice as the reference lattice on which atoms can move. The lattice constant of the DSC lattice is smaller than that of the crystals on both sides of the boundary. We found that the grain boundary changes into the liquid-like high temperature phase at the temperature range much below the bulk melting point.

We have extended these findings and have worked on a three-dimensional grain boundary, as reported in Appendix B. The work is an ABC-CBA stacking boundary in a fcc crystal. The reference lattice has three times as many lattice points as the fcc lattice of concern. The basic cluster of the CVM method is a three-layer rhombus prism with twelve lattice points. Since the structure is three-dimensional, the number of variables is large (about 90,000). Nevertheless, the natural iteration method<sup>6</sup> can solve the set of simultaneous nonlinear algebraic equations. For computation a CRAY computer, which is capable of vector processing, was used.

The calculation leads to thermodynamic information about the boundary: the excess free energy, the entropy and the density profile. Additional work is planned for different temperatures and chemical potentials, and for (110) and (112) directions of the boundary. Thus far, however, only two temperatures for the (110) boundary have been calculated, and further commentary on the noteworthy features of this boundary would be premature.

(C) In Appendix C we have printed a still unpublished paper by Dr. John W. Cahn of the National Bureau of Standards who has been collaborating on this project. This paper concerns faceting and dissociation of grain boundaries and is expected to be an important work in the field.

## SECTION 2

### FIRST ORDER TRANSITIONS WITHIN ROTATIONAL APB's IN $L1_0$ PHASE

The CuAu-type ordered phase is called  $L1_0$  and is a layer structure with alternating Cu and Au layers. We placed these layers perpendicular to the plane of a paper to form the right-hand side of the boundary. We kept the layers perpendicular to the paper and turned them  $90^\circ$ , then placed them on the left-hand side of the boundary. The boundary formed is illustrated in Figure 1 of Appendix A.

We used the tetrahedron as the basic cluster and implemented the CVM<sup>2</sup> to calculate the boundary structure. The mathematical technique is similar to the one used before<sup>4</sup> in calculating the APB and IPB related to the  $Cu_3Au$  phase. The grand potential  $G$  of the entire system including the boundary region is minimized, keeping the chemical potentials fixed. The  $G$  quantity is defined as

$$G = F - \sum_i \mu_i N_i = E - TS - (\mu_1 N_1 + \mu_2 N_2) \quad , \quad (1)$$

where  $F$  is the Helmholtz free energy,  $E$  is the internal energy,  $S$  is the entropy,  $\mu_i$  is the chemical potential, and  $N_i$  is the total number of the  $i$ -th atom ( $i=1$  and  $2$ ). In minimizing  $G$ , we placed the end conditions for the far left and far right ends in the respective homogeneous state.

In the formulation we did not include vacancies or many-body interactions. Therefore, the results are symmetrical with respect to the interchange of 1 and 2 (Cu and Au) species. When we express  $\mu_1 - \mu_2$  simply as  $\mu$ , the stoichiometric composition (Cu and Au, both 50%) corresponds to  $\mu = 0$ . We may choose  $\mu > 0$  for the Au-rich side.

When we calculated the excess adsorption,  $\Gamma$ , of Au at the boundary, we discovered that a high temperature  $\Gamma$  is positive when  $\mu > 0$  and that  $\Gamma$  changes discontinuously to a negative value when  $\mu$  crosses  $\mu = 0$  to the  $\mu < 0$  side. This behavior shows that there are two phases coexisting at  $\mu = 0$  for this temperature and that the transition is first order. This behavior is shown in Figure 4(a) of Appendix A.

For the low temperature region, we derived the first order transition of a similar kind. However, the low temperature behavior is distinctly different from the high temperature one, as is discussed in detail in Section 4 of Appendix A; we can define a transition from the low to high temperature behavior at  $kT_3/|w| = 0.515$  in Figure 3 of Appendix A. The transition at  $T_3$  and at  $\mu = 0$  is a third order.

The behavior of this system around  $T_3$  satisfies all of the thermodynamic requirements. However, the theoretical results are so unique that we decided not to publish the findings at this time, but rather to spend more time examining the validity of the results.

Besides the first order transition discussed above, there is one more phase transition near the composition 0.54, as shown in Figure 5 of Appendix A. This phase transition is due to the order-disorder change within one of the Cu layers of the layer structure.

### SECTION 3

#### THEORY OF ABC-CBA STACKING BOUNDARY IN fcc STRUCTURE

The (111) planes of the fcc structure is stacked as ABCABC... as opposed to the ABAB... stacking of the hcp structure. A boundary in the fcc structure is formed when the stacking is ABC... on the left-hand side and CBA... on the right. We discuss the structure of this stacking boundary in Appendix B.

Atoms were not only allowed to be located on fcc lattice points, but also at interstitial positions. The interstitial positions are defined by translating the fcc lattice perpendicular to the (111) direction, as shown in Figure 2 of Appendix B. Including these interstitial positions, the reference lattice forms a hexagonal lattice which has three times as many lattice points as the original fcc lattice. This hexagonal lattice plays the role of the reference DSC lattice used in the two-dimensional grain boundary examinations discussed in Ref. 5.

The basic cluster is the three-layer rhombus prism (defined in the reference hexagonal lattice), as shown in Figure 4 of Appendix B. The subclusters, V2, U3, U2, P3 and P2, shown in Figure 4, are also used.

In the reference hexagonal lattice, atomic pairs on adjacent lattice pairs are excluded. The second-neighbor atomic pair is the stable pair and is assigned an attractive potential energy,  $-\epsilon$  ( $\epsilon$  being positive). The potential energy assignment for atomic pairs is defined in Table 1 of Appendix B. The 0-9 pair is stable in the fcc structure and the 0-8 pair is stable in the hcp structure. In view of our work on the fcc we assigned an attraction to 0-9 and a repulsion to 0-8.

The entropy expression based on the rhombus prism is one of the key points in the formulation. It is derived by using the standard derivation of the entropy expression in the CVM.<sup>7</sup>

The equilibrium state is derived by minimizing the grand potential, which is of the form of Equation (1), the difference being that  $N_1$  is the total number of atoms in a system,  $\mu_1$  is the chemical potential of the atoms, and  $\mu_2 = 0$ . We impose the end condition where the left end of the system is in the homogeneous ABC stacking state and the right end is the CBA stacking state.

Since the number of independent variables is about 90,000, it is necessary to use a fast computer. A CRAY computer, which has vectorization capability, solved the variables by the iteration method in about 50 min CPU time.

The density profile across the boundary is shown in Figure 6 of Appendix B for the (110) boundary orientation.

In order to derive useful information from the computation, it is necessary to work out several different temperatures for at least two orientations of the boundary. Further work along this line is being planned.

#### SECTION 4

##### TRANSITIONS AND PHASE EQUILIBRIA AMONG GRAIN BOUNDARY STRUCTURES

The geometry of a grain boundary is characterized by three angular variables,  $R$ , and two angular variables,  $N$ . The  $R$  variables specify the misorientation of the two grains meeting at the boundary, and the  $N$  variables are for the normal to the boundary plane. The excess free energy,  $\gamma$ , depends on  $R$  and  $N$ . Recently, Dr. John W. Cahn, our consultant and collaborator, noted that the relation between  $\gamma$  and  $N$  is analogous to the relation between the bulk Helmholtz free energy and the composition. When this analogy is extended, the well-established concept and formulation of phase equilibria of bulk systems can be translated into the new concept and formulation of phase and phase equilibria among grain boundaries. In this way, Cahn has developed a theory of grain boundary faceting and dissociation. This is a pioneering and novel idea in the field of grain boundary physics and will undoubtedly open up new activities.

Dr. Cahn kindly agreed to have this unpublished work printed in this report as Appendix C. (The work was done at the National Bureau of Standards. However, the research in Ref. 40 was supported by this contract, as acknowledged at the end of the paper.)

#### ACKNOWLEDGMENT

In carrying out this contract, the invaluable help and consultation of Dr. John W. Cahn of the National Bureau of Standards is cordially acknowledged.



#### REFERENCES

1. C.M. van Baal, *Physica* 64, 571 (1973).
2. R. Kikuchi, *J. Chem. Phys.* 60, 1071 (1974).
3. J.W. Cahn and R. Kikuchi, *Acta Met.* 27, 1329 (1979).
4. R. Kikuchi and J.W. Cahn, *Acta Met.* 27, 1337 (1979).
5. R. Kikuchi and J.W. Cahn, *Phys. Rev.* B21, 1893 (1980).
6. R. Kikuchi, *J. Chem. Phys.* 65, 4545 (1976).
7. M. Kurata, R. Kikuchi, and T. Watari, *J. Chem. Phys.* 21, 434 (1953).

## APPENDIX A

### First order transition within rotational APB's in $L1_0$ phase\*

Ryoichi Kikuchi

Hughes Research Laboratories

#### ABSTRACT

The  $90^\circ$  rotational antiphase boundaries (APB) in the  $L1_0$  phase (CuAu-type ordered phase in the fcc lattice) are studied using the tetrahedron approximation of the cluster variation method. Calculation is done for a nearest-neighbor interaction without many-body forces. At the stoichiometric composition, excess adsorption of Au at the boundary increases discontinuously as the boundary changes from Cu-rich to Au-rich isothermally, indicating a first order transition. There is another first order transition at a larger Au composition. The nature of the transitions is shown by plotting profiles of densities on four sublattices.

\* Supported by U.S. Army Research Office.

## A. INTRODUCTION

Properties of boundaries in the fcc lattice were studied before<sup>1</sup> using the tetrahedron as the basic cluster in the cluster variation method (CVM).<sup>2,3</sup> Calculations were done on the antiphase boundaries (APB) in the  $A_3B$  phase ( $L1_2$ ) and on the interphase boundaries (IPB) between the  $L1_2$  and the disordered ( $A3$ ) phase. The excess free energies due to the IPB and APB showed a marked feature in that they go through maxima as the temperature increases.

In the present paper, we apply the same tetrahedron treatment of the CVM to APBs in the AB-type phase ( $L1_0$ ) in the fcc lattice. The main part of the paper is concerned with the boundary illustrated in Figure 1, which is drawn for the Au-Cu alloy. The  $L1_0$  phase has a layer structure of Au-rich and Cu-rich planes alternating with each other. A line in Figure 1 indicates a crystal plane that is perpendicular to the plane of the paper. We see that the left side of the boundary is rotated by  $90^\circ$  with respect to the right side. Since the layer planes on the left side are  $90^\circ$  to the direction of the boundary, we may call this the  $90^\circ$ -rotational boundary.

As shown in (A) and (C) in Figure 1, two cases are distinguishable, depending on whether the layer closest to the boundary on the right-side phase is Au-rich, as in (A), or Cu-rich, as in (C).

## B. GRAND POTENTIAL MINIMIZATION

We can distinguish four sublattices. We number the lattice planes as shown in Figure 1. The odd sublattices I and III are on odd planes. We use the index  $i=1$  for a Cu atom and  $i=2$  for a Au atom. The probability that a I sublattice point at position  $n$  is occupied by the  $i$ -th species is written as  $x_{I,n}(i)$ . Since vacancies are not considered in the formulation,  $x$ 's are normalized for any  $n$  and for  $\alpha = I, II, III, \text{ and } IV$  as

$$x_{\alpha,n}(1) + x_{\alpha,n}(2) = 1 \quad . \quad (1)$$

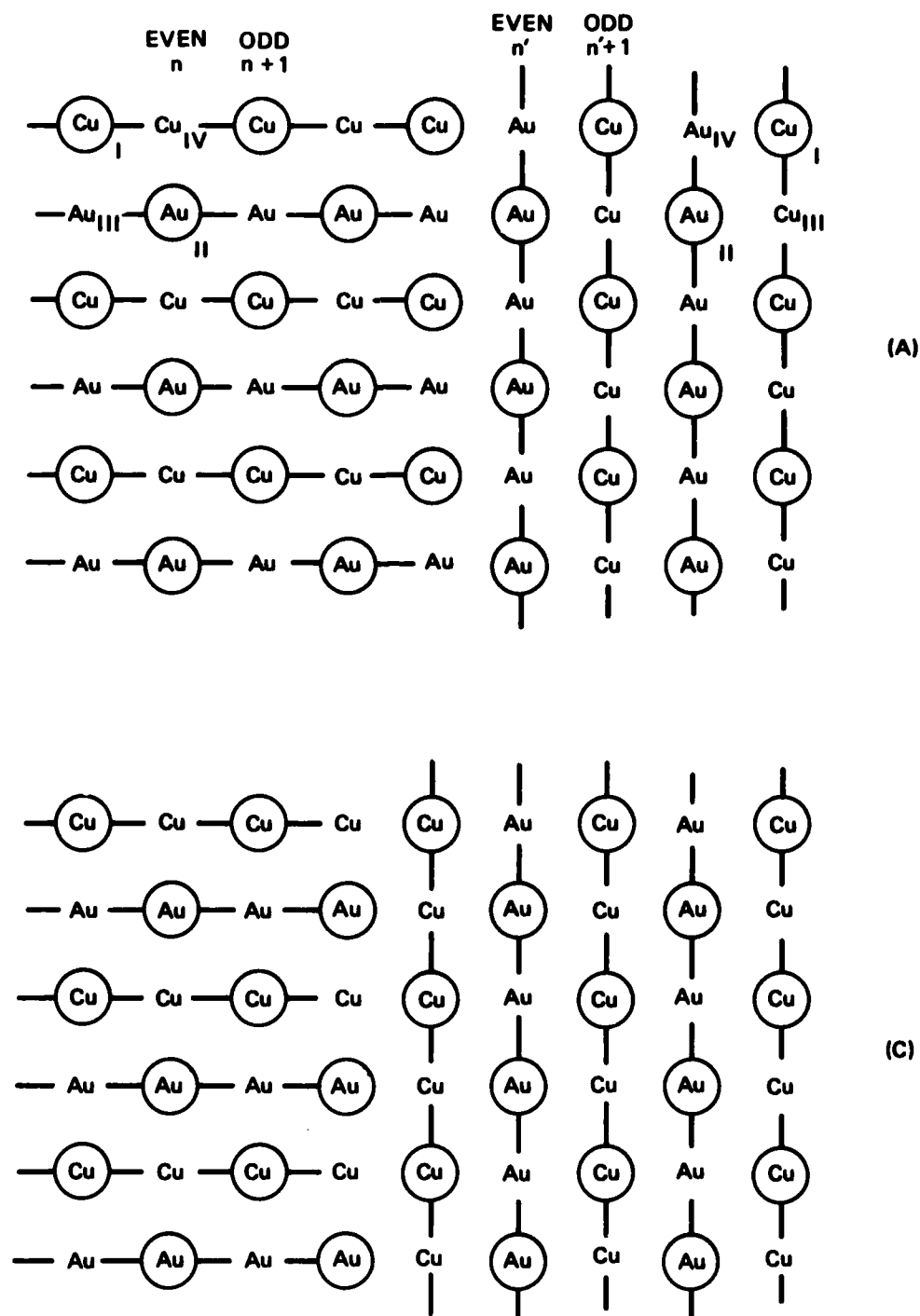


Figure 1. Structure of the  $90^\circ$ -rotational APB. The Au and Cu layers are perpendicular to the plane of the paper. In (A), the Au layer on the right is closest to the boundary, while in (C), the Cu layer is closest to the right.

As was done in the previous work on the fcc boundaries,<sup>1</sup> we use as the basic cluster a tetrahedron made of four adjacent lattice points. There is one kind of tetrahedron for each  $n$ . Since each lattice point is occupied either by Cu or Au, there are 16 possible configurations of a tetrahedron. Probabilities of these configurations are used as the basic variables, which we will call the  $z$  variables.

In order to solve the equilibrium structure of the boundary, we first write the grand potential  $G$  in terms of the  $z$  variables, and then minimize  $G$  with respect to  $z$ 's.

The grand potential  $G$  is defined as

$$G = E - TS - (\mu_1 N_1 + \mu_2 N_2) \quad , \quad (2)$$

where  $E$  is the internal energy,  $S$  is the entropy,  $\mu_i$  ( $i=1$  and  $2$ ) is the chemical potential of the  $i$ -th species and  $N$  is the total number of the  $i$ -th atoms in the system.

The energy is written based on the values for nearest neighbor pairs. Without the loss of generality we can assign the energy value 0 for the  $i$ - $i$  pair ( $i = 1$  or  $2$ ) and  $w$  for the  $1$ - $2$  pair, as was done in Ref.1. The many-body interaction parameters,  $\alpha$  and  $\beta$ , used in Ref.1 however, are made equal to zero in the present paper in order to simplify computations, and because the inclusion of  $\alpha$  and  $\beta$  does not change the qualitative features of the results.

The entropy expression is the key element of the CVM. It is written in terms of the  $z$  variables and of the probabilities for subclusters, namely, lattice pairs and lattice points. Triangles are subclusters of a tetrahedron, but do not appear in the entropy expression of the tetrahedron treatment. There are six different kinds of lattice pairs for each  $n$ , depending on how the four sublattices are connected.

In writing the chemical potential terms in Equation (2), when we do not include vacancies in the lattice, the sum of  $\mu_1$  and  $\mu_2$  vanishes so that we define the independent  $\mu$  as

$$\mu_1 = \mu_2 \equiv \mu \quad . \quad (3)$$

Due to the symmetry of the problem,  $\mu = 0$  at the 50-50 composition, and  $\mu$  increases with the Au composition.

The equilibrium structure of the boundary is derived by minimizing the grand potential  $G$ , keeping  $T$  and  $\mu$  fixed, with respect to the tetrahedron variables under the normalization constraints, continuity constraints and the end structure constraints. The continuity constraints guarantee that two  $z$ 's on adjoining position share a lattice pair. For the left end conditions we require that  $x_I(i) = x_{IV}(i)$  and  $x_{II}(i) = x_{III}(i)$  take the bulk values of the Cu and Au sublattices, respectively. For the right end,  $x_I(i) = x_{III}(i)$  and  $x_{II}(i) = x_{IV}(i)$  take the corresponding values. These choices are in accordance with the Figure 1 assignment.

Differentiations of  $G$  lead to simultaneous non-linear equations. They are solved by the natural iteration method (NIM), which has been developed before.<sup>4</sup> Each tetrahedron has 16  $z$  variables. Typically, we work  $n$  (the position of the plane) ranging from 1 through 50, leading to the total 800  $z$  values. The continuity constraints require additional 150 Lagrange multipliers. In spite of the relatively large number of variables, the NIM converges well. The Lagrange variables are determined by the iteration scheme called the minor iteration.<sup>1</sup>

### C. BOUNDARY PROFILE

A typical profile is shown in Figure 2. This plots the occupation probability  $x(2)$  of a Au atom at a lattice point. The boundary is around the positions  $n \approx 20$  through 25.

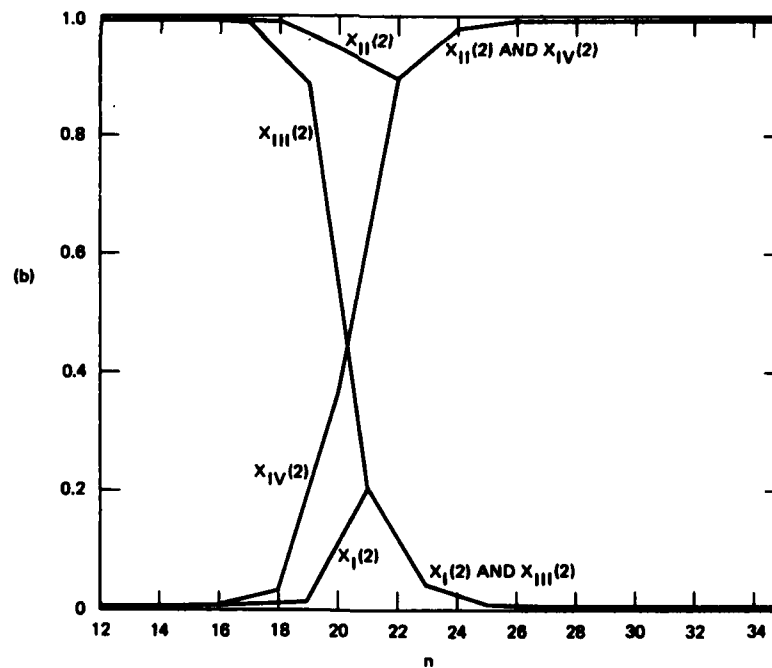
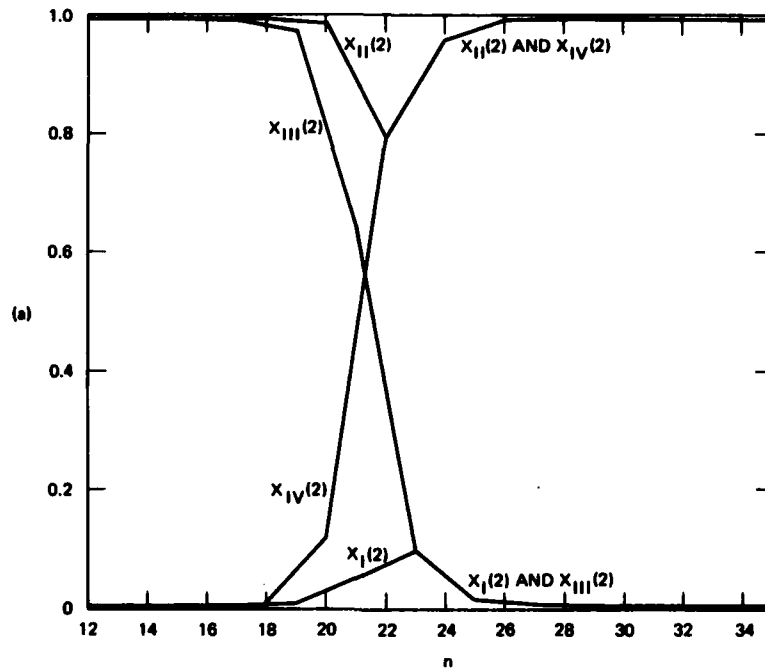


Figure 2. Density profile of Au atoms on the four sublattices across the boundary at  $kT/|w| = 0.7$ . The values are  $+0.02$  in (a) and  $-0.02$  in (b). (a) and (b) correspond to Figure 1 (A) and (C), respectively.

On the left end of Figure 2,  $x_{II}(2)$  and  $x_{III}(2)$  are practically the same and are close to unity. This means II and III sublattices are occupied preferentially by Au atoms in agreement with the sublattice assignment in Figure 1. As we come closer to the boundary,  $x_{II}(2)$  and  $x_{III}(2)$  gradually deviate from each other, as do  $x_I(2)$  and  $x_{IV}(2)$ .

The structure of the sublattice occupation on the right side of the boundary is different. At and beyond the position  $n=22$ ,  $x_{II}(2)$  and  $x_{IV}(2)$  are exactly equal. The two values split off suddenly at  $n=20$ . Similarly,  $x_I(2)$  and  $x_{III}(2)$  are equal at and beyond  $n=23$ , and split off at  $n=21$ .

We now see the difference of the right and left sides of the boundary. Coming from the right, II and IV split suddenly, while on the left, II and III gradually deviate from each other. The difference is understood based on the fact that II and IV are on the same plane parallel to the boundary, while II and III are on different planes.

Coming from the right in Figure 2(a),  $n=22$  is the last position at which the Au sublattices II and IV are the same. Since this point appears often in the subsequent discussions, let us call it the branching point and write it as  $n_{br}(Au) = 22$ . From the splitting of I and III sublattices we can write that  $n_{br}(Cu) = 23$ . At the  $n_{br}(Au)$  position, the plane is a Au-rich layer, and at  $n_{br}(Cu)$  the plane is Cu-rich. Since  $n_{br}(Au) < n_{br}(Cu)$  in Figure 2(a), we see that this is the structure of Figure 1(A) rather than 1(C). Let us call this the A-type boundary, implying that a Au-layer is next to the boundary. The boundary of Figure 1(C) will be called the C-type boundary.

#### D. TRANSITION FROM A- TO C-TYPE BOUNDARY

The boundary structure is either the A-type or C-type and not in between. Therefore, we expect a transition between the two types. In the present formulation many-body interaction is excluded and thus the system is symmetric with



respect to the interchange of Cu and Au. This means the transition from A- to C-type boundary occurs at the 50-50 composition or at  $\mu = 0$ .

Figure 3 plots the excess amount of Au atoms adsorbed at the boundary region in the A-type boundary at the 50-50 composition. The value of  $\Gamma_{\text{Au}}$  in Figure 3 is per one lattice point (for the area of  $a^2$ ) in a plane parallel to the boundary. At the same composition, the plot of excess Au atoms in the C-type boundary is a mirror image of the Figure 3 curve with respect to the center vertical line.

Figure 4(a) plots schematically the excess free energy  $\sigma$  of the boundary at a constant temperature against  $\mu$ . Note:

$$-\frac{\partial \sigma}{\partial \mu} = \Gamma_{\text{Au}} - \Gamma_{\text{Cu}} \quad (4)$$

Since both the A-type and C-type boundaries exist at the same composition and at the same temperature, and since  $\partial \sigma / \partial \mu$  changes discontinuously as the C-type boundary changes to the A-type at  $\mu = 0$ , the transition is of the first order.

The curve in Figure 3 crosses the center vertical line at about  $kT_3/|w| = 0.515$ . At this temperature the  $\Gamma_{\text{Au}}$  remains zero when we go from the C-type boundary to the A-type boundary, and hence the transition is accidentally third order.

Below  $T_3$  the transition is again first order, but the curves behave differently, as shown in Figure 4(b).

Figure 5 shows another demonstration of the transition. The example is at  $kT/|w| = 0.7$ . As we see in Figure 2(a) and (b), the Au branching point at this temperature is placed at  $n_{\text{br}}(\text{Au}) = 22$ . Solid curves in Figure 5 are  $x_{\text{I}}(2)$  and  $x_{\text{III}}(2)$  at  $n=21$ , which is the point one lattice plane to the left of  $n_{\text{br}}(\text{Au})$ . In Figure 2(a),  $x_{\text{I}}(2)$  and  $x_{\text{III}}(2)$  are split at  $n=21$ , while they are together there in Figure 2(b). Figure 5 shows this behavior by the splitting of  $x_{\text{I}}(2)$  and  $x_{\text{III}}(2)$  at  $x(2)=0.5$ .

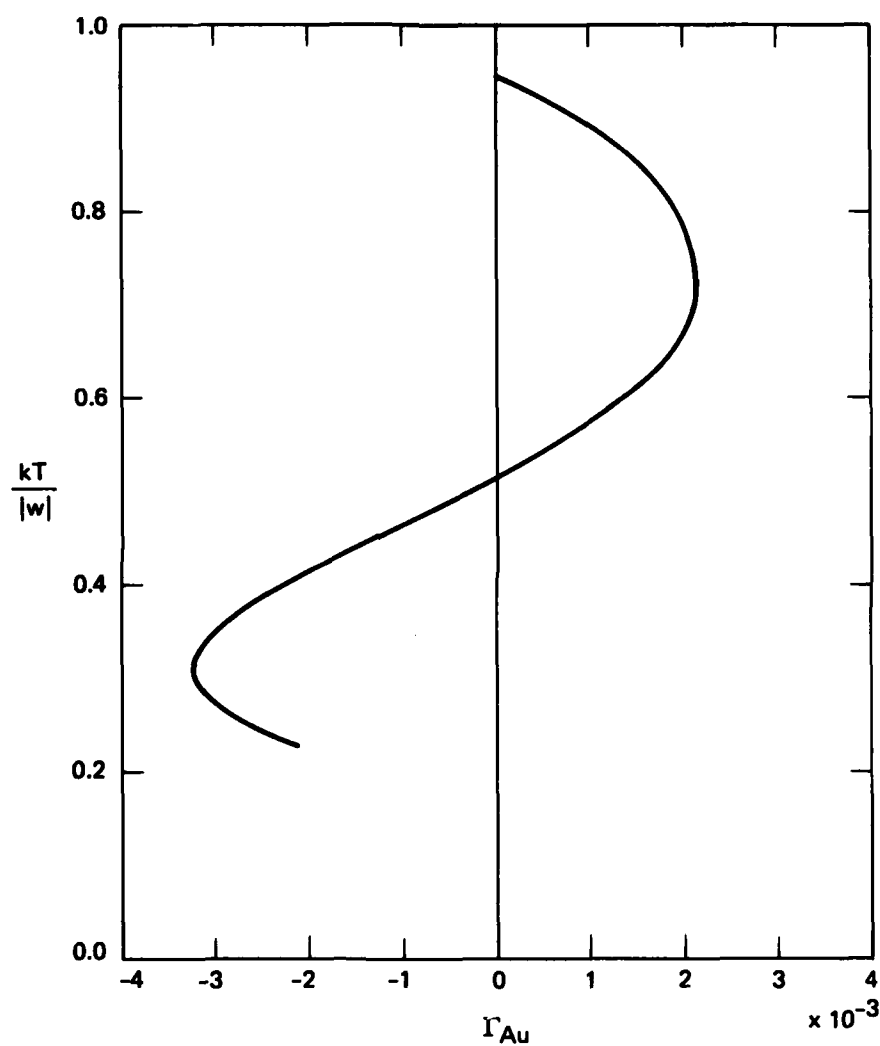


Figure 3. Adsorption of Au atoms at the boundary plotted against temperature. The curve is on one branch of the free energy surface corresponding to Figure 1 (A).

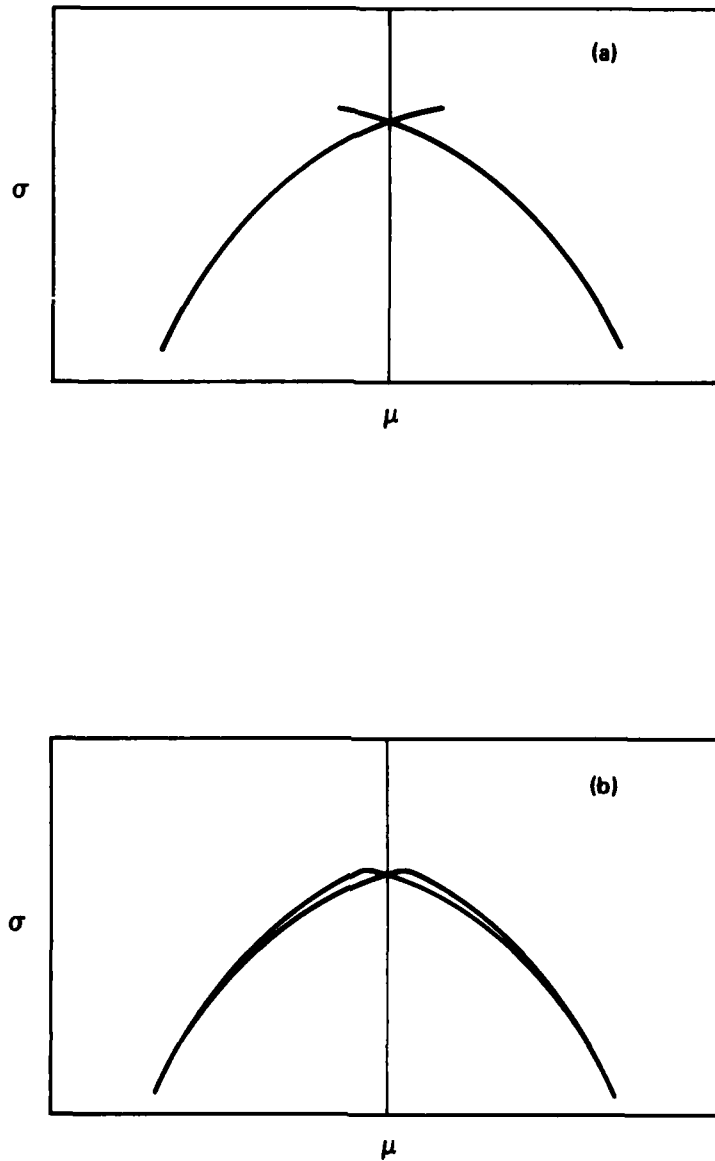


Figure 4. Schematic diagram of  $\sigma$  versus  $\mu$  at a constant temperature. (a) is for  $T$  above  $T_3$ , and (b) is below.

Figure 5 indicates another phase transition at about  $x(2)=0.54$ . For  $x(2) < 0.54$  the branching positions are  $n_{br}(Au) = 22$  and  $n_{br}(Cu)=23$ . For  $x(2) > 0.54$ , the latter shifts to  $n_{br}(Cu)=25$ , as shown in Figure 6. It is worth noting that I and III sublattices on the  $n=23$  plane are split, although the plane is sandwiched between the two planes,  $n=22$  and  $n=24$ , on which II and IV sublattices are the same.

#### E. DISCUSSION

Figure 7 plots the excess Au atoms,  $\Gamma_{Au}$ , against the composition at  $kT/|w|=0.7$ . There are small gaps at  $x(2)=0.5$ ,  $0.542$ , and  $0.458$ , and they correspond to the two phase transitions discussed in Section 4 and displayed in Figure 5.

Figure 8 plots the excess free energy  $\sigma$  due to the boundary at the 50-50 composition against temperature. This curve is to be compared with Figures 6 and 10 of Ref. 1. The curves in Figure 8 are monotonically increasing as  $T$  decreases, since this is for a constant  $\mu(=0.0)$ . If we plot  $\sigma$  for a constant composition, other than  $x(2)=0.5$ , we expect a maximum at a finite temperature.

For general information, Figure 9 shows  $\mu$  versus  $x(2)$  at  $kT/|w|=0.7$ .

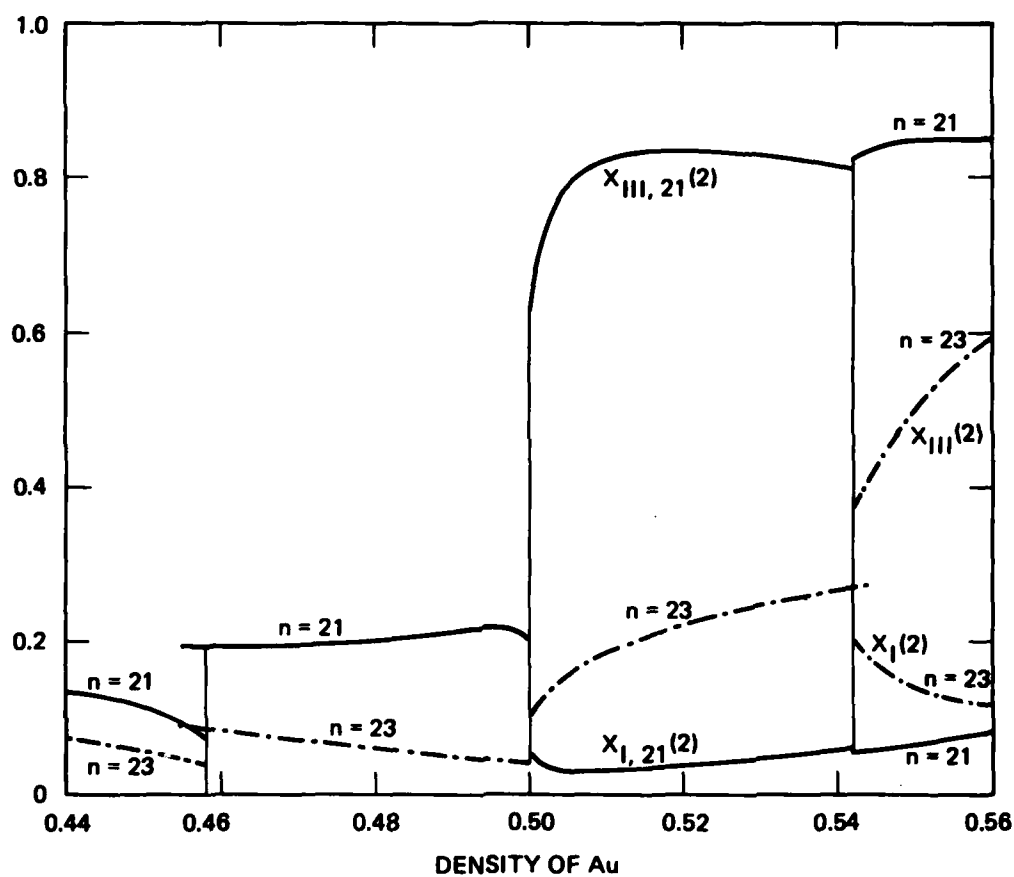


Figure 5. The Au density,  $x(2)$ , on sublattices I and III plotted against the Au density in the bulk phase at  $kT/|w| = 0.7$ . Discontinuities at  $x(2) = 0.50$  and  $0.542$  indicate phase transitions.

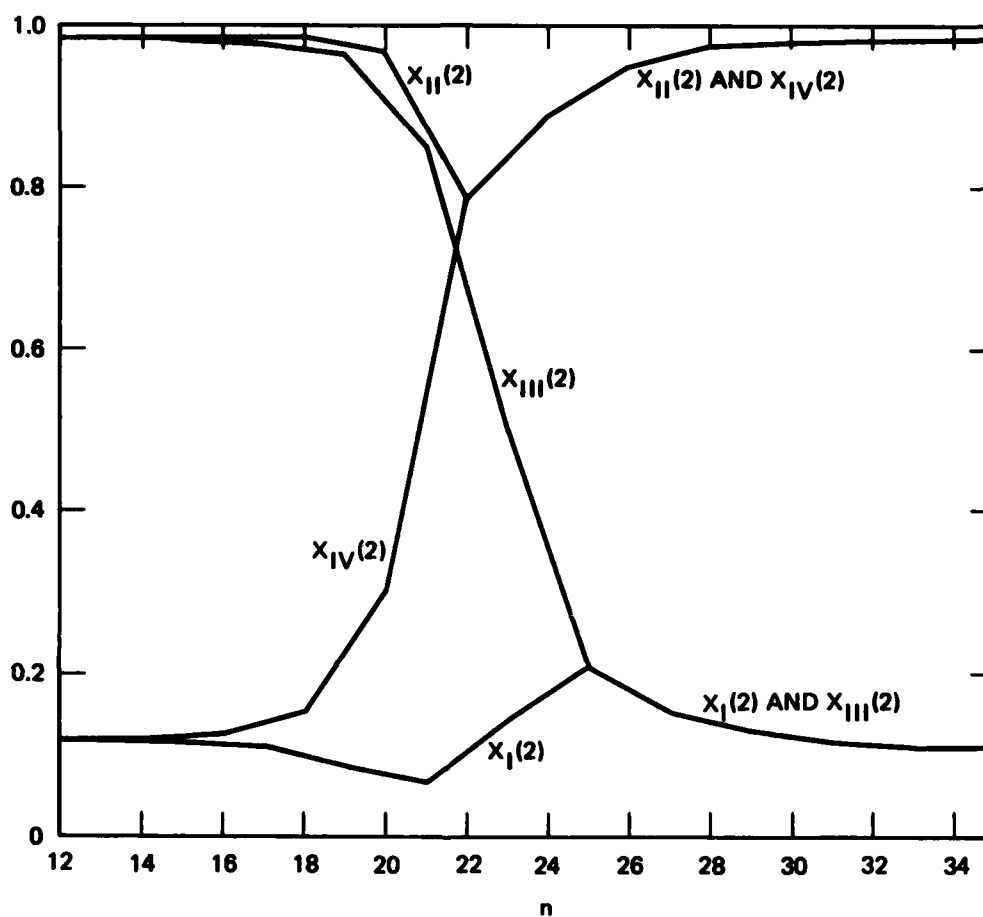


Figure 6. Density profile of Au atoms on the four sublattices across the boundary at  $kT/|w| = 0.7$  and for  $\mu = 1.3$ . The overall density of Au throughout the system is 0.549.

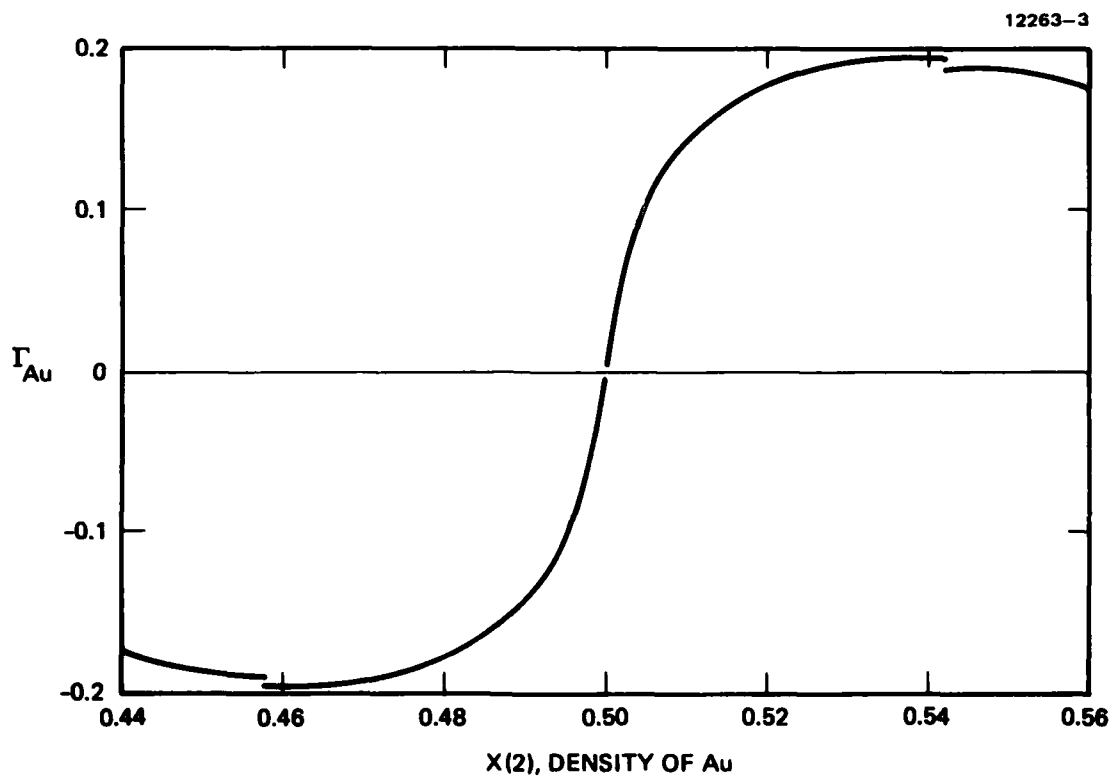


Figure 7. The excess Au adsorbed at the surface against the overall density of Au throughout the system. The temperature is  $kT/w = 0.70$ .

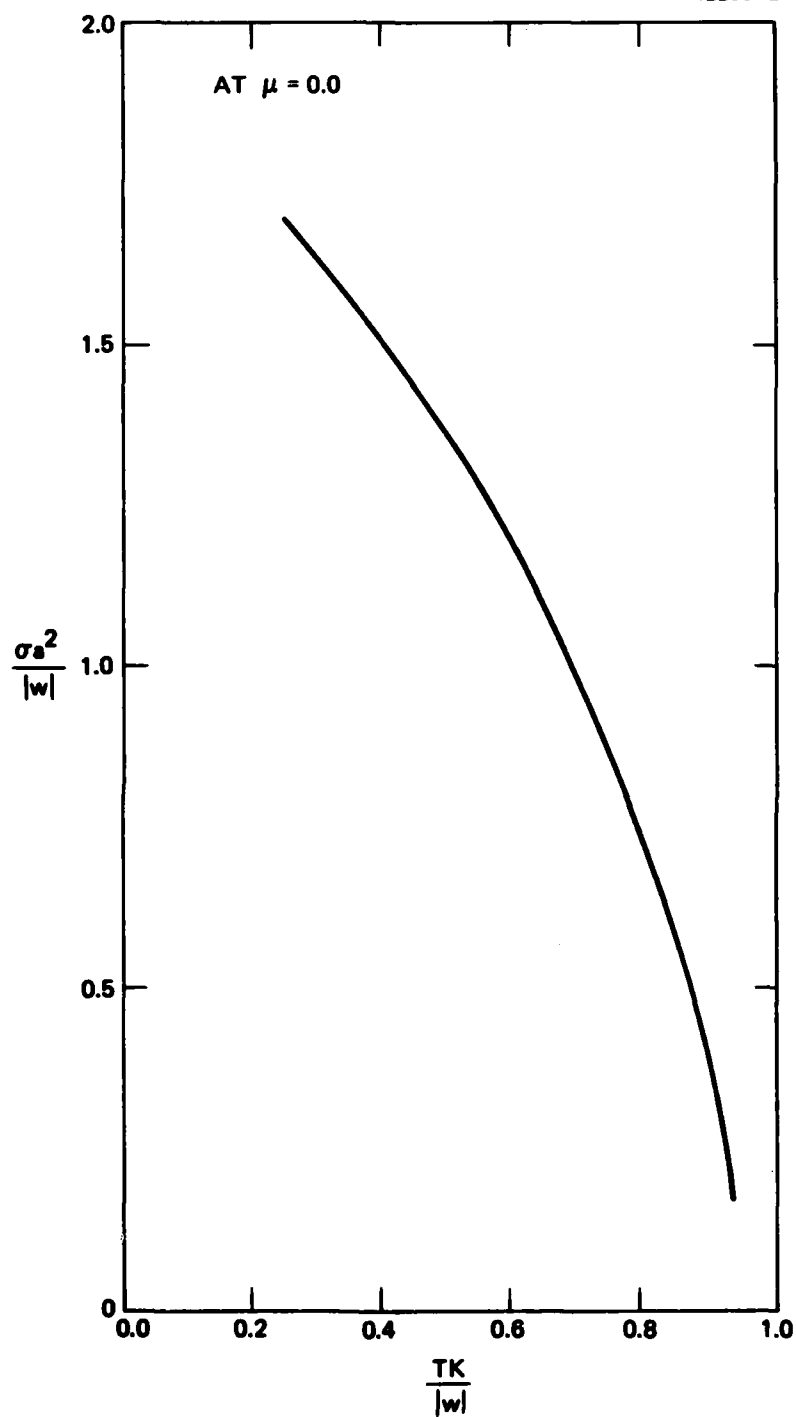


Figure 8. The excess free energy  $\sigma$  at the stoichiometric composition plotted against temperature. Within a crystal plane parallel to the boundary the area per lattice point is written as  $a^2$ .



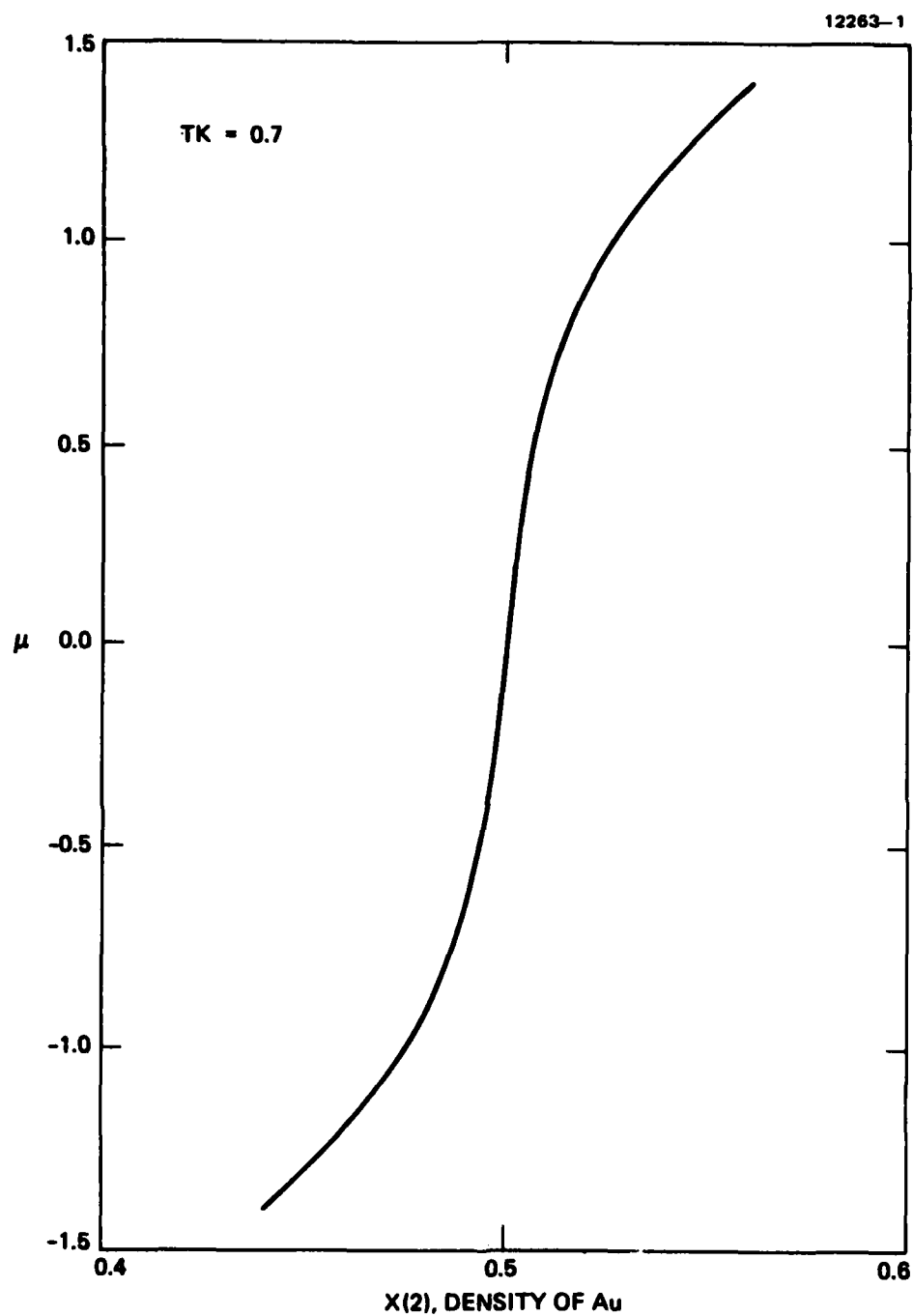


Figure 9. The chemical potential  $\mu$  plotted against the density of Au in the bulk homogeneous phase.

REFERENCES

1. R. Kikuchi and J.W. Cahn, Acta Met. 27, 1337 (1979).
2. R. Kikuchi, Phys. Rev. 81, 988 (1951).
3. R. Kikuchi, J. De Phys. 38, C7, 307 (1977).
4. R. Kikuchi, J. Chem. Phys. 60, 1071 (1974).

## APPENDIX B

### THEORY OF ABC-CBA STACKING BOUNDARY IN fcc STRUCTURE\*

Ryoichi Kikuchi

Hughes Research Laboratories

#### ABSTRACT

In the fcc lattice a boundary is formed when the stacking is ABC... on the left-hand side and CBA... on the right-hand side. The structure of this boundary is calculated using the cluster variation method (CVM). A hexagonal lattice is used as the reference lattice; the original fcc lattice occupies 1/3 of the reference lattice. A three-layer rhombus prism is chosen as the basic cluster of the CVM. The grand potential of the entire system, including the boundary region, is minimized with respect to the basic variables. The set of simultaneous nonlinear algebraic equations for 90,000 variables is solved iteratively using a CRAY computer. Properties of the boundary, including the excess free energy and the density profile across the boundary, are obtained. The calculation done so far is for one temperature and for the (110) orientation. Calculations for more temperatures and for (112) orientation are being planned.

\*Supported by U.S. Army Research Office.

## 1. Introduction

In a series of papers,<sup>1-4</sup> we have theoretically studied structures of phase boundaries. The theoretical method we used has been the cluster variation method (CVM).<sup>5</sup> One of the most recent works in the series has been the study of a two-dimensional grain boundary<sup>4</sup> in which we discovered that the boundary changes from the low-temperature crystalline state into a high-temperature liquid-like state at a temperature region much below the bulk melting temperature. In the study we used a square DSC lattice as the reference lattice, and worked with a model where atoms in the stable crystalline structure occupy one out of five DSC lattice points.

This paper is an extension of Ref. 4 and is the first attempt to calculate the three-dimensional grain boundary. The model we will use can be briefly summarized as follows. The fcc structure has the ABCABC... stacking while the hcp has an ABAB... stacking. In the fcc lattice, when the left-hand side has the ABC... stacking and the right-hand side the CBACBA... stacking, a boundary is formed between the two sides. The structure of this boundary is the subject of our concern here.

Goodhew, Tan, and Balluffi<sup>6</sup> reported an experimental study of this boundary. We will supplement these experiments and will elucidate the structure of the boundary.

## 2. Model

The (111) plane of the fcc lattice is a two-dimensional triangular sublattice, which is called B. We supplement this sublattice, B, by two more sublattices, A and C, which are linear translations of B, as shown in Figure 1. We call the (111) plane of Figure 1 layer 1, and the (111) plane above it layer 2. In layer 2 the lattice points are directly above the C position and we supplement them by A and B triangular sublattices, as shown on the left-hand side of Figure 2. The A lattice points in layer 3 are similarly supplemented by points B and C. Together, lattice points A, B, and C form the reference lattice on which atoms can be located.

In Figure 2, A, B, and C sublattices are marked with a circle, a square, and a triangle, respectively, and the original fcc lattice points are indicated by filled marks. The left-hand side is the ABC... stacking and the right-hand side is the CBA... stacking. The center of the boundary is indicated by broken lines.

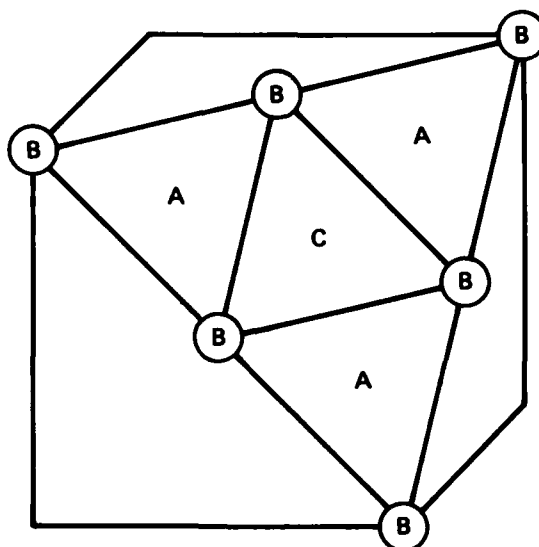


Figure 1. The reference lattice points A, B, and C on the layer "1" of the fcc lattice

The interaction energies are assumed to be as indicated in Table 1. When an atom is at 0, no atoms can come to points 1 or 4. The distances 0-2 and 0-5 are the same and are the nearest-neighbor distance of the original fcc lattice.

In order to treat the ABC-CBA boundary problem of our present interest, it is necessary to include the third layer interaction and distinguish the ABC and ABA stackings. For this purpose we include the 0-8 and 0-9 interactions, as in Table 1. The 0-9 interaction is favored for the fcc stacking, and the 0-8 is favored for the hcp stacking. Since our system is fcc, we choose the parameter  $\epsilon_F > 0$  (attraction) and  $\epsilon_H < 0$  (repulsion).

In formulating the mathematics of the problem we number the lattice planes parallel to the boundary as  $n-1, n, n+1, \dots$ , as shown in Figure 2. On each plane we distinguish nine sublattice points  $\kappa=1, \dots, 9$  as shown in Figure 2. The point  $\kappa=1$  on layer 1 is marked by a circle and  $\kappa=2$  by a square, and so on. Note that vertical to the layer shown in Figure 2, the circle points form a line, while the square points form a line of their own, and the triangle points form a line of their own. Thus, for example, on the plane  $n$ , a  $\kappa=4$  point is about a  $\kappa=1$  point.

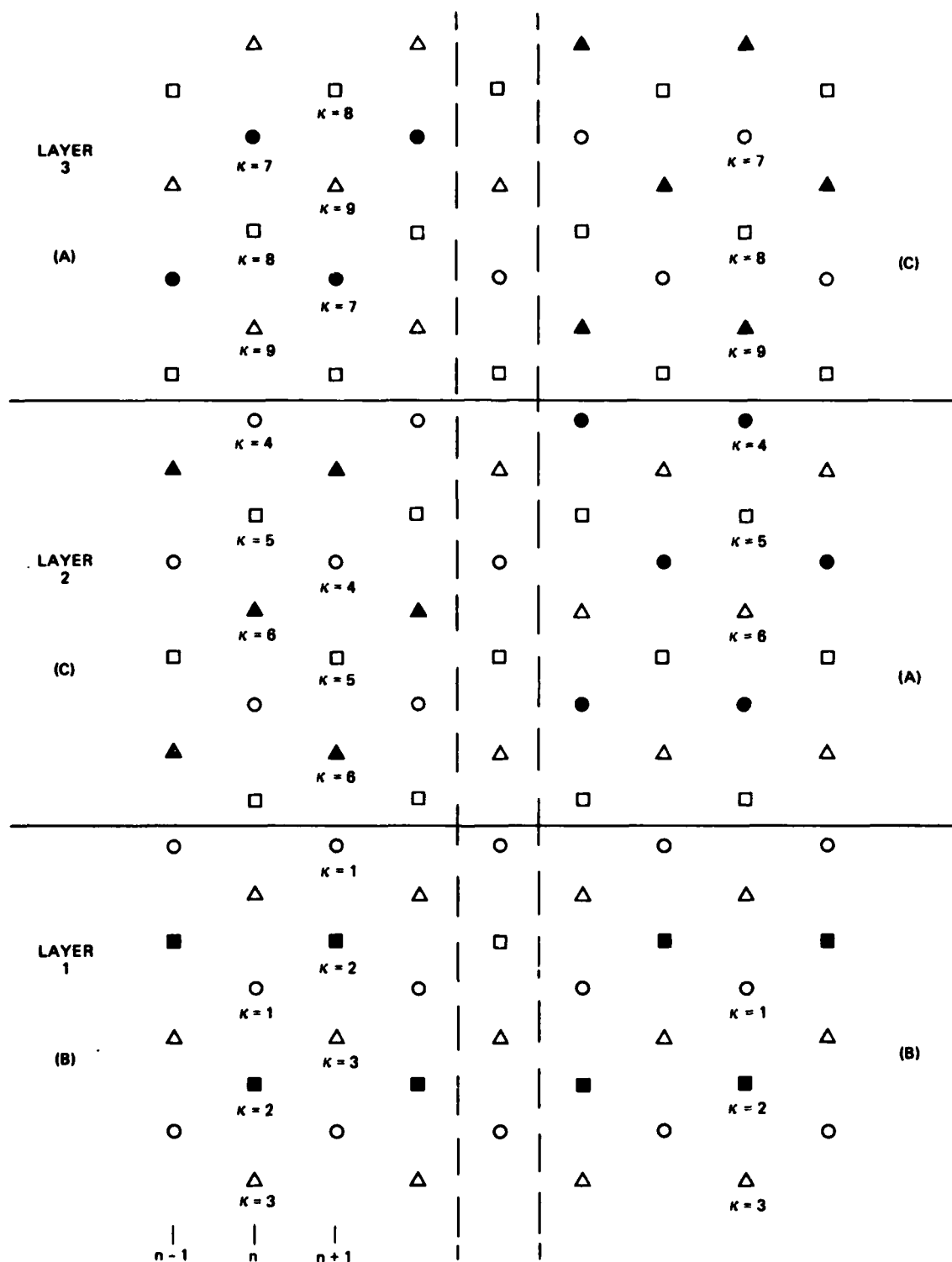
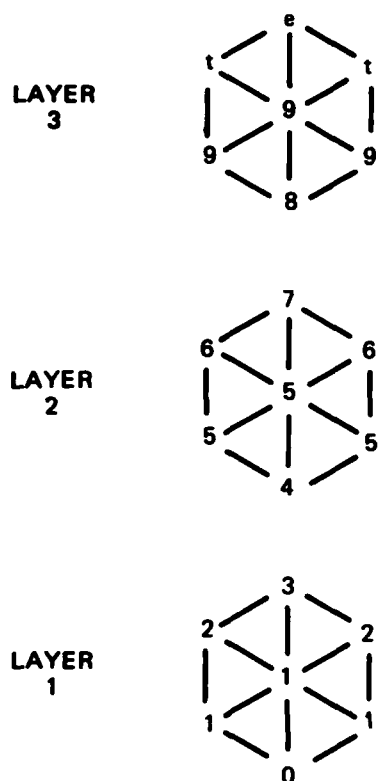


Figure 2. The ABC and CBA stackings in the fcc lattice.

Table 1. Definition of the Interaction Potentials

12263-17



PAIR	ENERGY
0-e	0
0-t	0
0-9	$-\epsilon\epsilon_F$
0-8	$-\epsilon\epsilon_H$
0-7	0
0-6	0
0-5	$-\epsilon$
0-4	EXCLUDED
0-3	0
0-2	$-\epsilon$
0-1	EXCLUDED

The boundary plane in Figure 2(a) is parallel to the (110) plane of the fcc lattice. Another boundary shown in Figure 3 parallel to the (112) plane can also be formulated using a similar technique and will be reported later.

### 3. Variables

In treating this problem using the CVM we have chosen a three-layer rhombus prism as the basic cluster. It is true that a three-layer hexagon prism leads to a better approximation, but it was not used because it would need larger memory space in computers. The variables we use in the formulation are illustrated in Figure 4.

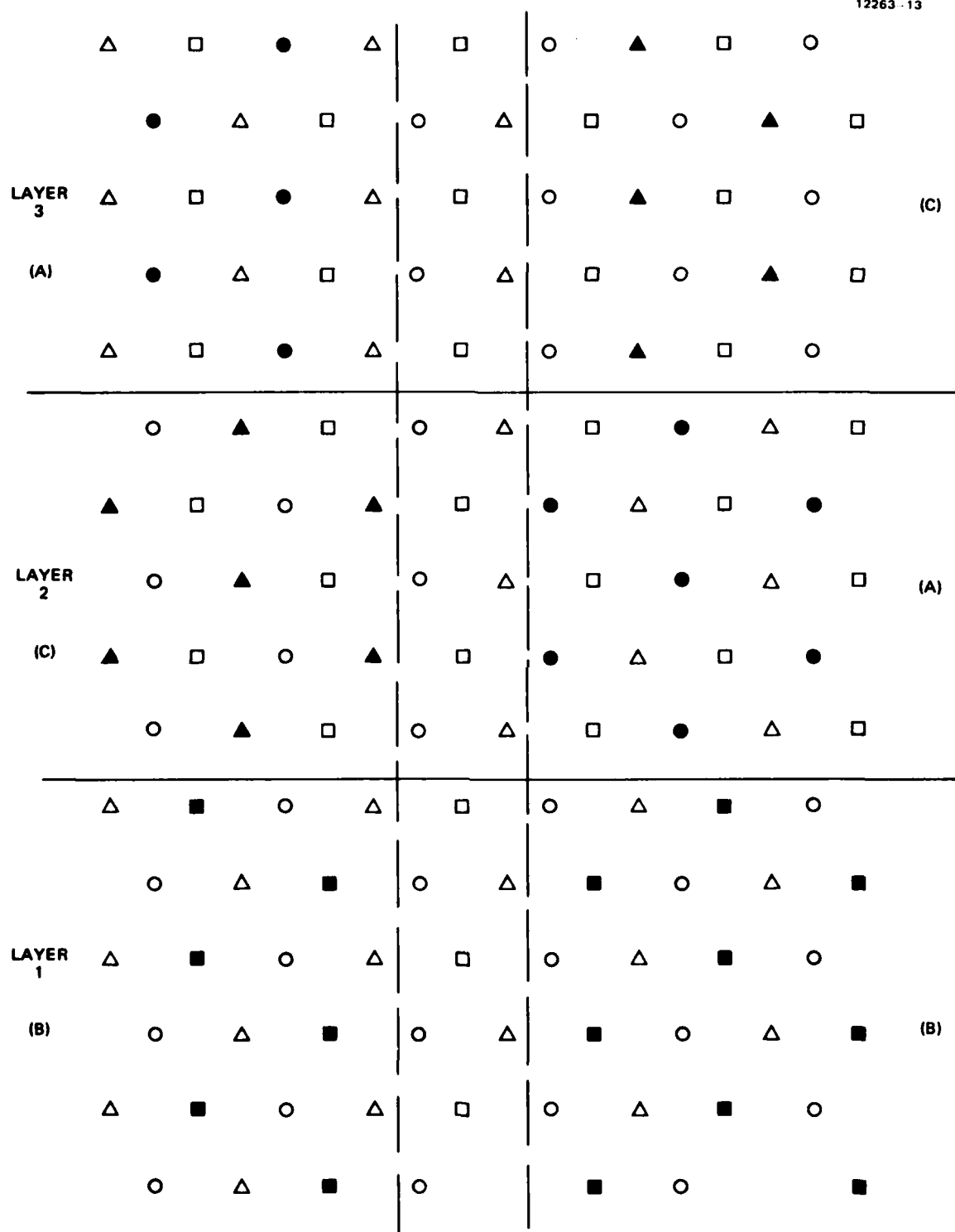


Figure 3. The (112) boundary corresponding to Figure 2.



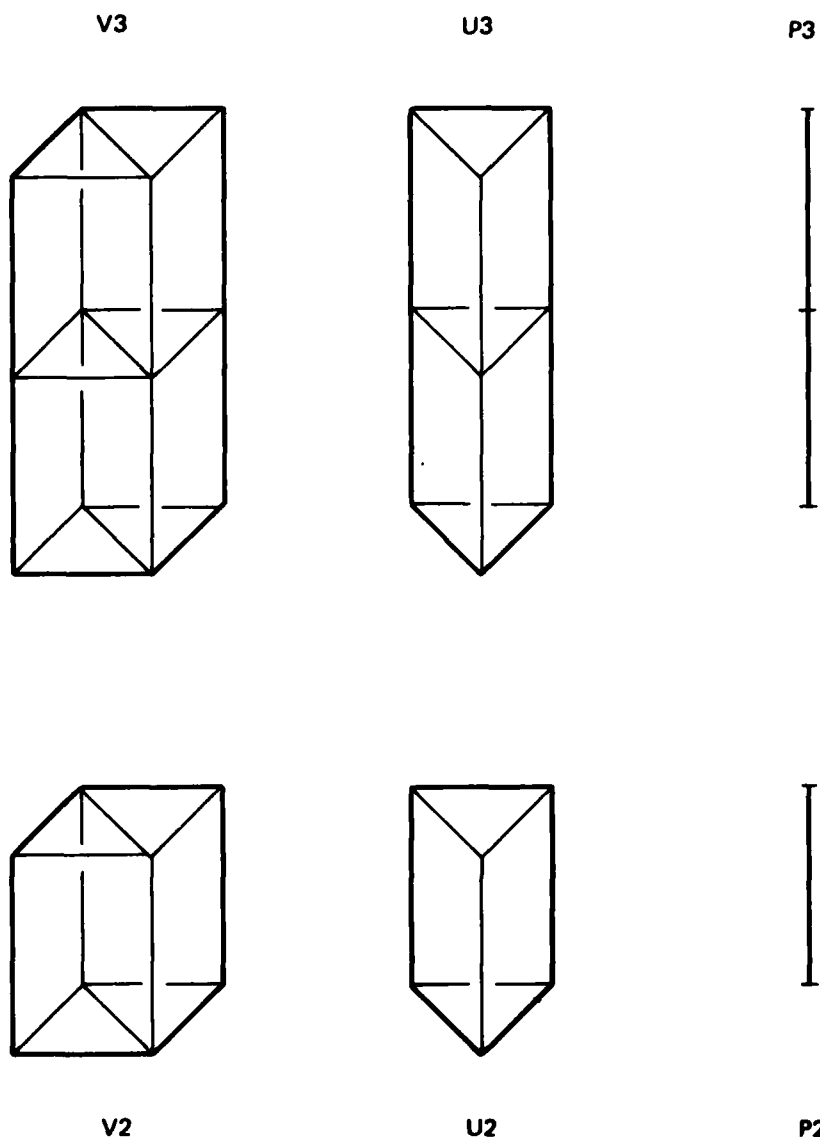


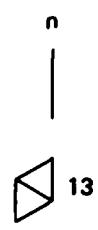
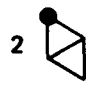
















Figure 4. The shapes of the clusters used in the CVM treatment.

a. V2 and V3 Variables. Configurations of a rhombus are numbered as in Table 2. Note that we distinguish three orientations of the rhombus: left-tilted, horizontal, and right-tilted. Using the numbers in Table 2, we write the probability variable of a three-layer rhombus prism as  $V3_{n,\kappa;i,j,k}$ . The subscripts  $i$ ,  $j$ , and  $k$  take one of the numbers in Table 2,  $i$  being for the bottom layer configuration, and  $j$  and  $k$  for the middle and top layers, respectively. A rhombus has two diagonals. The two points at the ends of the longer diagonal lie on the same  $k$  lattice points in Figure 2. The subscript  $k$

Table 2. The Definitions of the Rhombus Configuration Numbers. A dot represents an atom.

12263-18

n	n	n
1 	7 	13 
2 	8 	14 
3 	9 	15 
4 	10 	16 
5 	11 	17 
6 	12 	18 

is this  $\kappa$  number for the end points of the longer diagonal. Because the orientations of the three rhombi (on the three layers) of a prism are the same, we have a restriction on the  $i, j$ , and  $k$  that all three numbers are in one of the three columns in Table 2; numbers of different columns of Table 2 do not mix.

Because of the exclusion requirement in Table 1, when the bottom layer has configuration 2 (in Table 2) the middle layer cannot be 2 or 6. This exclusion relation is written in Table 3.

Table 3. The Exclusion Matrix  
MXCLV ( $I, J$ )

12263-19

ABOVE <sub>j</sub> BELOW <sub>i</sub>	1	2	3	4	5	6
1						
2		X				X
3			X			X
4				X		
5					X	
6		X	X			X

[MXCLV]<sub>i,j</sub>

In addition to the  $V3$  variables we use  $V2_{n,k;i,j}$  for the 2-layer rhombus prism. The meaning of the subscripts are similar to those for  $V3$ .

The precise definition of the  $V3$  variable is that out of  $N$  rhombi of the  $(n,k)$  kind, the number of rhombi which have the configuration  $(i,j,k)$  is  $V3_{n,k;i,j,k}$ .

The  $V2$  variables can be evaluated when the  $V3$  variables are given as

$$V2_{n,k;i,j} = \sum_k V3_{n,k;i,j,k} = \sum_k V3_{n,kM3;k,i,j} \quad , \quad (3.1)$$

where  $kM3$  is the  $k$ -number of the lattice point one layer below  $k$ , and is calculated as

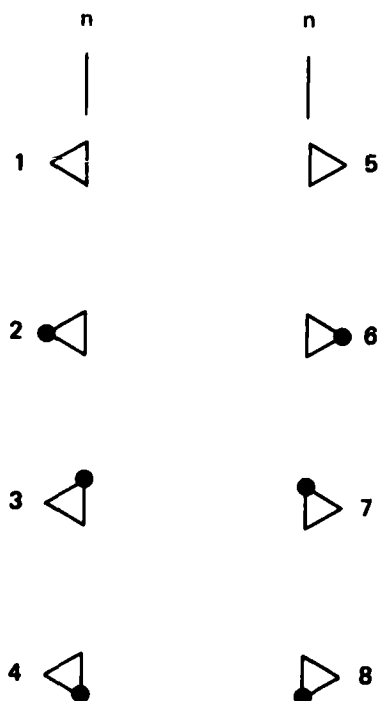
$$kM3 = \text{MOD}(k + 5, 9) + 1 \quad . \quad (3.2)$$

b. V2 and V3 Variables. There are two triangle orientations, left-pointing and right-pointing. The configurations of a triangle are numbered in Table 4. The probability variables for the three-layer triangle prism are written as  $V_{3n,k;i,j,k}$ , where  $k$  is for the left or right tip of the triangle. The subscripts  $i, j$ , and  $k$  are for the configuration of Table 4, and no numbers on different columns of Table 4 mix. The exclusion requirements corresponding to Table 3 are

$$i \neq j \text{ and } j \neq k \text{ except } i = j = 1 \text{ and } j = k = 1 \quad . \quad (3.3)$$

Table 4. The Definition of the Triangle Configuration Numbers. A dot represents an atom.

12263-20



For the two-layer triangle prism, we define  $V2_{n,k;i,j}$ . They are derived from  $V3$ 's by

$$V2_{n,k;i,j} = \sum_k V3_{n,k;i,j,k} = \sum_k V3_{n,kM3;k,1,j} \quad , \quad (3.4)$$

where  $kM3$  is defined in (3.2).

c. P2 and P3 Variables. These variables are defined in Table 5. The exclusion requirements are the same as in (3.3). The reduction relations similar to (3.3) hold.

Table 5. The Definition of the Pair and Triplet Variables. A dot is an atom.

12263-21

$P2_{n,\kappa;i,j}$	$P3_{n,\kappa;i,j,k}$
1,1	1,1,1
2,1 •	2,1,1 •
1,2 •	1,2,1 •
	1,1,2 •
	2,1,2 •

d. Reduction of U3 from V3. The variable  $V3_{n,k;i,j,k}$  can be derived from either of the three orientations of V3. As a preparation of this reduction we write the relations among two-dimensional triangles (written as  $x_{n,k;l}$ ) in Table 4 and two-dimensional rhombi (written as  $y_{n,k;i}$ ) in Table 2. They are

$$\begin{aligned} x_{n,k;l} &= \sum_{i=1}^6 [XLYL]_{l,i} y_{n-1,kp2;i} \\ &= \sum_{i=1}^6 [XLYC]_{l,i} y_{n,k;i+6} \quad \text{for } l=1,\dots,4 \quad (3.5a) \\ &= \sum_{i=1}^6 [XLYR]_{l,i} y_{n,kp1;i+12} \end{aligned}$$

for the left-pointing triangle, and

$$\begin{aligned} x_{n,k;l+4} &= \sum_{i=1}^6 [XRYL]_{l,i} y_{n,kp1;i} \\ &= \sum_{i=1}^6 [XRYC]_{l,i} y_{n,k;i+6} \quad \text{for } l=1,\dots,4 \quad (3.5b) \\ &= \sum_{i=1}^6 [XRYR]_{l,i} y_{n+1,kp2;i+12} \end{aligned}$$

for the right-pointing triangle. The matrices  $[ ]_{l,i}$  are defined in Table 6. The subscript  $kp1$  and  $kp2$  are defined as

Table 6. The Definition of the Matrices to Connect Rhombus Configurations (i) to Triangle Configurations ( $\ell$ )

12263-22

$\ell \backslash i$	1	2	3	4	5	6
1	1	1				
2				1		
3					1	
4			1			1

$$[XLYL]_{\ell,i} = [XRYR]_{\ell,i}$$

$\ell \backslash i$	7	8	9	10	11	12
1	1		1			
2		1				1
3				1		
4					1	

$$[XLYC]_{\ell,i}$$

$\ell \backslash i$	13	14	15	16	17	18
1	1		1			
2					1	
3		1				1
4					1	

$$[XLYR]_{\ell,i} = [XRYL]_{\ell,i}$$

$\ell \backslash i$	7	8	9	10	11	12
5	1	1				
6			1			1
7				1		
8					1	

$$[XRYC]_{\ell,i}$$

$$kP1 = k + 1 ,$$

$$\text{except } kP1 = k - 2 \text{ when } \text{MOD}(k,3) = 0 , \quad (3.6a)$$

and

$$kP2 = k - 1 ,$$

$$\text{except } kP2 = k + 2 \text{ when } \text{MOD}(k,3) = 1 . \quad (3.6b)$$

Using the matrices defined in Table 6, we can write the reduction relations of U3's from V3's as

$$\begin{aligned} U3_{n,k;\ell,m,n} &= \sum_{i,j,k=1}^6 [XLYL3]_{\ell,m,n;i,j,k} V3_{n-1,kP2;i,j,k} \\ &= \sum_{i,j,k=1}^6 [XLYC3]_{\ell,m,n;i,j,k} V3_{n,k;i+6,j+6,k+6} \quad (3.7) \\ &= \sum_{i,j,k=1}^6 [XLYR3]_{\ell,m,n;i,j,k} V3_{n,kP1;i+12,j+12,k+12} , \end{aligned}$$

where we define

$$[XLYL3]_{\ell,m,n;i,j,k} = [XLYL]_{\ell;i} [XLYL]_{m;j} [XLYL]_{n;k} , \quad (3.8)$$

and similar relations for [XLYC3] and [XLYR3]. In the subscripts of U3 on the left-hand side of Equation (3.7), n appears twice, first for the lattice location and then for the triangle index (n=1,...,4), but no confusion is expected. In Equation (3.7)  $\ell, m$  and  $n$  are from 1 through 4.



The relations corresponding to (3.5b) are

$$U_{n,k;l+4,m+4,n+4}^3 = \sum_{i,j,k=1}^6 [XLYR3]_{l,m,n;i,j,k} V_{n,kPl;i,j,k}^3 \quad (3.9)$$

and two more expressions.

e. Reduction of P3 from V3. The variables, P3's, can be written as linear combinations of V3's. For example,

$$P_{n,k;l,m,n}^3 = \sum_{i,j,k=1}^6 [PV2]_{l,m,n;i,j,k} V_{n,k;i,j,k}^3 \quad (3.10)$$

This is for the top lattice point where the atom sits in configuration 2 on the left column of Table 2. We can write similar relations for configurations 2, 3, and 4 of Table 2 using matrices [PV3], [PV4], and [PV5]. These matrices are defined in Table 7.

#### 4. Grand Potential

The mathematical procedure of calculating the equilibrium state is to minimize the grand potential,  $G$ , keeping the chemical potential fixed. The function  $G$  is defined as

$$G = E - TS - \mu N_A \quad (4.1)$$

where  $\mu$  is the chemical potential and  $N_A$  is the total number of atoms in a system.

a. Energy E. Calculation of the energy is defined in detail in the model in Section 2. Using the V3 variables, the energy,  $E$ , is written as follows:

$$E = N \sum_n \sum_{k=1}^9 \sum_{i,j,k=1}^6 \epsilon_{i,j,k} \sum_{m=0,6,12} V_{n,k;i+m,j+m,k+m}^3 \quad (4.2)$$

where  $N$  is the number of three-layer units in a system.

Table 7. The Matrices which connect Rhombus Configurations (i) to Triplet Configurations (l)

12263-23

$\ell \backslash i$	1	2	3	4	5	6	
1	1		1	1	1		[PV2] $_{\ell; i}$
2		1				1	

$\ell \backslash i$	1	2	3	4	5	6	
1	1	1		1	1		[PV3] $_{\ell; i}$
2			1			1	

$\ell \backslash i$	1	2	3	4	5	6	
1	1	1	1		1	1	[PV4] $_{\ell; i}$
2				1			

$\ell \backslash i$	1	2	3	4	5	6	
1	1	1	1	1		1	[PV5] $_{\ell; i}$
2					1		

The parameter,  $\epsilon_{i,j,k}$ , is the energy per rhombus and is made of three parts:

$$\epsilon_{i,j,k} = \epsilon_i^{(1)} + \epsilon_j^{(1)} + \epsilon_k^{(1)} + \epsilon_{ij}^{(2)} + \epsilon_{jk}^{(2)} + \epsilon_{ik}^{(3)}, \quad (4.3)$$

where  $\epsilon_i^{(1)}$  is the energy within a layer,  $\epsilon_{ij}^{(2)}$  is the energy between adjacent layers, and  $\epsilon_{ik}^{(3)}$  is the energy between the first and third layers.

The energy due to the diagonal pair of a rhombus (for the  $i=6$  case in Table 2) is counted in three V3's (appearing in three different layers of a V3).

Thus

$$\epsilon_i^{(1)} = \frac{1}{3} \epsilon \delta_{i6}. \quad (4.4)$$

A pair-wise interaction,  $\epsilon$ , between adjacent layers (for the pair 0-5 in Table 1) is counted ten times. Thus

$$\epsilon_{ij}^{(2)} = \frac{1}{10} \epsilon (ED)_{ij}, \quad (4.5)$$

where the matrix,  $(ED)_{ij}$ , is defined in Table 8.

The third layer interaction,  $\epsilon_{ik}^{(3)}$ , is due to either  $-\epsilon\epsilon_F$  or  $-\epsilon\epsilon_H$  in Table 1. The vertical bond,  $-\epsilon\epsilon_H$ , is counted 12 times: 4 times in the rhombus of one of the three orientations (Table 2). The fcc-type interaction,  $-\epsilon\epsilon_F$ , is counted 5 times, i.e., a half of  $\epsilon_{ij}^{(2)}$ . Thus, we write

$$\epsilon_{ik}^{(3)} = \frac{1}{12} \epsilon\epsilon_H (EH)_{ik} + \frac{1}{5} \epsilon\epsilon_F (ED)_{ik}, \quad (4.6)$$

where both matrices are defined in Table 8.

Table 8. The Energy Matrices (ED) for Adjoining Layers and (EH) for the First-Third Layers

12263-24

ABOVE $j$ BELOW $i$	1	2	3	4	5	6
1						
2				1	1	
3				1	1	
4		1	1		1	2
5		1	1	1		2
6				2	2	

MATRIX (ED)<sub>ij</sub>

ABOVE $k$ BELOW $i$	1	2	3	4	5	6
1						
2		1				1
3			1			1
4				1		
5					1	
6		1	1			2

MATRIX (EH)<sub>ik</sub>

b. Entropy S. The CVM entropy expression based on the three-layer rhombus prism can be derived from the entropy expression for the two-dimensional triangular lattice based on a rhombus cluster. The latter was derived previously<sup>7</sup> as

$$e^{S/k} = \frac{\{\text{Pair}\}^2}{\{\text{Rhombus}\} \{\text{Point}\}} \left[ \frac{\{\text{Triangle}\}^2}{\{\text{Rhombus}\} \{\text{Pair}\}} \right]^c, \quad (4.7)$$

where  $c$  is an integer. When the diagonal pair of the rhombus does not contribute to the potential energy, the ratio inside  $[ ]^c$  becomes unity. When the diagonal pair does contribute, as in the present case, we should use  $c = 2$ . Thus, in the present case, the basic relation is

$$e^{S/k} = \frac{\{\text{Triangle}\}^4}{\{\text{Rhombus}\}^3 \{\text{Point}\}}. \quad (4.8)$$

The entropy expression for the three-layer rhombus prism is then derived as

$$e^{S/k} = \frac{\{3\text{-l.tr.pr.}\}^4}{\{3\text{-l.rh.pr.}\}^3 \{3\text{-l.triplet}\}} : \frac{\{2\text{-l.tr.pr.}\}^4}{\{2\text{-l.rh.pr.}\}^3 \{2\text{-l.doublet}\}}, \quad (4.9)$$

where we abbreviated  $l$ , = layer, rh. = rhombus, pr. = prism, and tr. = triangle.

Writing in full, we obtain

$$\begin{aligned}
 S = kN \sum_n \sum_{k=1}^9 \left[ - \sum_{i,j,k=1}^6 \sum_{m=0}^2 \mathcal{L}(V^3_{n,k;i+6m,j+6m,k+6m}) \right. \\
 + \sum_{i,j=1}^6 \sum_{m=0}^2 \mathcal{L}(V^2_{n,k;i+6m,j+6m}) \\
 + 2 \sum_{i,j,k=1}^4 \sum_{m=0}^1 \mathcal{L}(U^3_{n,k;i+4m,j+4m,k+4m}) \\
 - 2 \sum_{i,j=1}^4 \sum_{m=0}^1 \mathcal{L}(U^2_{n,k;i+4m,j+4m}) \\
 \left. - \sum_{i,j,k=1}^2 \mathcal{L}(P^3_{n,k;i,j,k}) + \sum_{i,j=1}^2 \mathcal{L}(P^2_{n,k;i,j}) \right],
 \end{aligned}
 \tag{4.10}$$

where we define

$$\mathcal{L}(X) \equiv X \mathcal{L}_n X - X \quad .
 \tag{4.11}$$

In Equation (4.10),  $N$  is the number of three-layer units in a system as it was in Equation (4.2).

c. Chemical Potential Term. In the chemical potential term,  $-\mu N_A$  in (4.1), we need the number of atoms,  $N_A$ , which we write as follows. Each atom is counted 12 times in a 3-layer rhombus prism of one orientation (left-tilted, horizontal, or right-tilted, as in Table 1). Therefore,

$$N_A = N \sum_n \sum_{k=1}^9 \sum_{i,j,k=1}^6 \frac{1}{36} (A_i + A_j + A_k) \sum_{m=0}^3 V^3_{n,k;i+6m,j+6m,k+6m}, \quad (4.12)$$

where  $A_i$  is the number of atoms in the rhombus configuration ( $i = 1, \dots, 6$ , in Table 2), and is defined as

$$\begin{aligned} A_i &= 0 & \text{for} & \quad i = 1 \\ A_i &= 1 & \text{for} & \quad i = 2, 3, 4 \text{ and } 5 \\ A_i &= 2 & \text{for} & \quad i = 6 \end{aligned} \quad (4.13)$$

## 5. Basic Equations

The equilibrium state of the boundary is derived by minimizing the grand potential,  $G$ , and keeping the chemical potential,  $\mu$ , fixed. In so doing, several comments are in order.

a. Choice of Independent Variables. We choose the  $V3$  variables for the basic cluster as independent. Other variables,  $V2$ ,  $U3$ ,  $U2$ ,  $P3$  and  $P2$ , are all for the subclusters of the basic cluster and can be written as linear combinations of the  $V3$  variables, as was shown in Section 3.

b. Constraints on the Independent Variables. Although we choose  $V3$ 's as the independent variables in minimizing  $G$ , not all  $V3$ 's are actually independent. The mutual relations to be satisfied among  $V3$ 's are of three kinds. The example of the first kind is the equality in Equation (3.1). The constraints of the second kind come from the three ways of writing  $V3$ , as in Equation (3.7), and additional three ways in Equation (3.9). The third-kind of constraint is the normalization relations:

$$\sum_{i,j,k=1}^6 V3_{n,k;i+6m,j+6m,k+6m} = 1 ,$$

$$\text{for each } n,k, \text{ and } m=0, 1 \text{ and } 2 . \quad (5.1)$$

In minimizing G with respect to V3's, we use the Lagrange multipliers,  $\alpha$ 's,  $\gamma$ 's and  $\lambda$ 's, for the three kinds of constraints.

c. The Basic Equations. The basic equations for V3s are written as follows (we use  $i,j,k=1,\dots,6$ ):

$$V3_{n,k;i,j,k} = \hat{V}3_{n,k;i,j,k} \exp(\beta\lambda) , \quad (5.2)$$

where the  $\exp(\ )$  factor is determined from the normalization relations in Equation (5.1). The un-normalized part,  $\hat{V}3$ , is written in two steps. In the first step we include the Lagrange multipliers,  $\alpha$ 's and  $\gamma$ 's, mentioned in b. above, and write

$$\begin{aligned} \ln \hat{V}3_{n,k;i,j,k} = & \ln \tilde{V}3_{n,k;i,j,k} - \alpha_{n,k;i,j} + \alpha_{n,kP3;j,k} \\ & - \sum_{\ell,m,n=1}^4 \left\{ \gamma_{LL}^{n+1,km2;\ell,m,n} [XLYL3]_{\ell,m,n;i,j,k} \right. \\ & \left. + \gamma_{RL}^{n,km1;\ell+4,m+4,n+4} [XLYR3]_{\ell,m,n;i,j,k} \right\} . \end{aligned} \quad (5.3)$$

The  $\tilde{V}3$  part does not include Lagrange multipliers, and is written as

$$\begin{aligned} \ln \tilde{V}3_{n,k;i,j,k} = & \beta \epsilon_{i,j,k} + \beta \mu (A_i + A_j + A_k) / 36 \\ & + \frac{1}{2} \ln V_{n,k;i,j,k} + \ln U_{n,k;i,j,k} - \frac{1}{4} \ln P_{n,k;i,j,k} \end{aligned} \quad (5.4)$$

The  $\epsilon_{i,j,k}$  term comes from the energy expression, and the A terms come from the chemical potential term; we define  $\beta = 1/kT$ . The last three  $\ln$  terms are



$$\begin{aligned}
\ell_{nV}{}_{n,k;i,j,k} &= \ell_n \left[ V^2_{n,k;i,j} V^2_{n,kP3;j,k} \right] \\
\ell_{nU}{}_{n,k;i,j,k} &= \sum_{\ell,m,n=1}^4 \left\{ [XLYL3]_{\ell,m,n;i,j,k} \ell_n \frac{U^3_{n,km2;\ell,m,n}}{[U^2_{n+1,km2;\ell,m} U^2_{n+1,km2P3;m,n}]^{1/2}} \right. \\
&\quad \left. + [XLYR]_{\ell,m,n;i,j,k} \ell_n \frac{U^3_{n,km1;\ell+4,m+4,n+4}}{[U^2_{n,km1,\ell+4,m+4} U^2_{n,km1P3;m+4,n+4}]^{1/2}} \right\} \\
\ell_{nP}{}_{n,k;i,j,k} &= \sum_{\ell,m,n=1}^2 [PV2]_{\ell,m,n;i,j,k} \ell_n \frac{P^3_{n,k;\ell,m,n}}{[P^2_{n,k;\ell,m} P^2_{n,kP3;m,n}]^{1/2}} \\
&\quad + [PV3]_{\ell,m,n;i,j,k} \ell_n \frac{P^3_{n+1,k;\ell,m,n}}{[P^2_{n+1,k;\ell,m} P^2_{n+1,kP3;m,n}]^{1/2}} \\
&\quad + [PV4]_{\ell,m,n;i,j,k} \ell_n \frac{P^3_{n,kP1;\ell,m,n}}{[P^2_{n,kP1;\ell,m} P^2_{n,kP1P3;m,n}]^{1/2}} \\
&\quad + [PV5]_{\ell,m,n;i,j,k} \ell_n \frac{P^3_{n+1,kP2;\ell,m,n}}{[P^2_{n+1,kP2;\ell,m} P^2_{n+1,kP2P3;m,n}]^{1/2}}
\end{aligned} \tag{5.5}$$

We derive similar expressions for  $\hat{V}^3_{n,k;i+6,j+6,m+6}$  and  $\hat{V}^3_{n,k;i+12,j+12,k+12}$ , but the exact equations will not be listed here. In the latter we use YLR and YRR corresponding to  $\gamma$ 's in Equation (5.3). The expression for  $\hat{V}^3_{n,k;i+6,j+6,m+6}$  contains all four kinds of  $\gamma$ .

## 6. Iterative Solution

We solve V3's from the basic equations and constraints using an iterative procedure called the natural iteration method (NIM).<sup>8</sup> The NIM is separated into the major iteration and the minor iteration.

a. The Major Iteration. (1) We start with the input values, V3's. (2) The subcluster variables V2, U3, U2, P3 and P2 are derived from V3 by the reduction procedure of Section 3. (3) Using (5.4) and (5.5), we calculate V3. (4) The un-normalized  $\hat{V}3$  in (5.3) is written using the Lagrange multipliers  $\alpha$ 's and  $\gamma$ 's. Using the minor iteration process to be explained in (b) below, the values of  $\alpha$ 's and  $\gamma$ 's are determined so that the constraints on  $\hat{V}3$ 's are satisfied. (5) After the minor iteration, the normalization factor,  $\lambda$ 's, are determined from Equations (5.2) and (5.1) to end up with the output, V3, of one major iteration step. This output is used as the input, V3, in step (1) above.

b. The Minor Iteration. We determine  $\alpha$ 's and  $\gamma$ 's in Equation (5.3) for the given  $\tilde{V}3$  in such a way that the first and second kinds of constraints mentioned in Section 5b. are satisfied. When we use Equation (5.2) in the first-kind constraint (3.1), we write

$$\begin{aligned} & \exp\left(-\alpha_{n,k;i+6m,j+6m}\right) \sum_{k=1}^6 \exp\left(\alpha_{n,k;i+6m,j+6m}\right) V_{n,k;i+6m,j+6m,k+6m}^3 \\ &= \exp\left(\alpha_{n,k;i+6m,j+6m}\right) \sum_{k=1}^6 \exp\left(-\alpha_{n,k;i+6m,j+6m}\right) V_{n,km3;k+6m,i+6m,j+6m}^3 \\ & \quad m = 0, 1 \text{ or } 2 \quad . \end{aligned} \tag{6.1}$$

Because V3's satisfy the normalization of Equation (5.1), we can choose  $\alpha$  for  $i=j=1$  as zero without the loss of generality:

$$\alpha_{n,k;1+6m,1+6m} = 0, \quad m = 0, 1 \text{ or } 2 \quad . \tag{6.2}$$

When we use Equation (6.2), we can eliminate the normalization factor,  $\lambda$ , by forming a ratio of Equation (6.1). We define

$$\begin{aligned} BL_{n,k;i+6m,j+6m} &\equiv \sum_{k=1}^6 \hat{v}_3_{n,k;i+6m,j+6m,k+6m} \\ BR_{n,k;i+6m,j+6m} &\equiv \sum_{k=1}^6 \hat{v}_3_{n,kM3;k+6m,i+6m,j+6m} \end{aligned} \quad (6.3)$$

Then we solve Equation (6.1) in the iterative form as

$$\begin{aligned} \alpha_{n,k;i+6m,j+6m}^{(out)} &= \alpha_{n,k;i+6m,j+6m}^{(in)} \\ &+ \frac{1}{2} b_{\alpha} \ell_n \left[ \frac{BL_{n,k;i+6m,i+6m} BR_{n,k;l+6m,l+6m}}{BL_{n,k;l+6m,l+6m} BR_{n,k;i+6m,j+6m}} \right], \end{aligned} \quad (6.4)$$

where  $b_{\alpha}$  is a damping factor. When  $b_{\alpha} = 0$ ,  $\alpha^{(out)}$  is equal to  $\alpha^{(in)}$ ;  $b_{\alpha} = 1$  is the case of no damping. In the actual computation we used  $b_{\alpha} = 1/4$ .

Using a procedure similar to the above for  $\alpha$ , we derive the minor iteration relations for  $\gamma$ 's as follows: In order to satisfy the two constraint equations in (3.7), we derive

$$\gamma_{LL}^{(out)}_{n,k;l,m,n} = \gamma_{LL}^{(in)}_{n,k;l,m,n} + \frac{1}{2} b_{\gamma} \ell_n \left[ \frac{GLLL_{n,k;l,m,n} GLLR_{n,k;l,l,l}}{GLLL_{n,k;l,l,l} GLLR_{n,k;l,m,n}} \right], \quad (6.5)$$

and

$$YLR_{n,k;l,m,n}^{(out)} = YLR_{n,k;l,m,n}^{(in)} + \frac{1}{2} b_Y \ln \left[ \frac{GLRL_{n,k;l,m,n}}{GLRL_{n,k;1,1,1}} \frac{GLRR_{n,k;1,1,1}}{GLRR_{n,k;l,m,n}} \right], \quad (6.5)$$

where we define

$$\begin{aligned} GLLL_{n,k;l,m,n} &\equiv \sum_{i,j,k=1}^6 [XLYL3]_{l,m,n;i,j,k} \hat{V}^3_{n-1,kP2;i,j,k} \\ GLRR_{n,k;l,m,n} &\equiv \sum_{i,j,k=1}^6 [XLYC3]_{l,m,n;i,j,k} \hat{V}^3_{n,k;i+6,j+6,k+6} \\ GLRL_{n,k;l,m,n} &\equiv \sum_{i,j,k=1}^6 [XLYR3]_{l,m,n;i,j,k} \hat{V}^3_{n,kP1;i+12,j+12,k+12} \\ GLRR_{n,k;l,m,n} &\equiv \sum_{i,j,k=1}^6 [XLYC3]_{l,m,n;i,j,k} \hat{V}^3_{n,k;i+6,j+6,k+6} \cdot (6.6) \end{aligned}$$

The coefficient,  $b_Y$ , in Equation (6.5) is a damping factor of similar nature as  $b_\alpha$  in Equation (6.4). In the actual calculations we used  $b_Y = 1/2$ .

We have two more constraint relations for  $V_3$  in the right-pointing triangle variables in Equation (3.9). These two constraints derive  $YRL$  and  $YRR$ , but the details are omitted.

## 7. Homogeneous Phase

Before calculating the boundary structure, we solve the equilibrium state of the homogeneous phase. We can use the same equations designed for the boundary and simply make the variables independent of the lattice location,  $n$ .

The homogeneous system is made up of three sublattices. Referring to Figure 2, the three are

$$\begin{aligned}\kappa_1 &= 1, 5, 9, \\ \kappa_2 &= 2, 6, 7, \\ \kappa_3 &= 3, 4, 8, \quad .\end{aligned}\tag{7.1}$$

When the temperature is very high, the three sublattices become equivalent and the system is disordered. For low temperatures when the sublattices are not equivalent, we can define the long-range order as the difference of the atomic densities on the lattices  $\kappa_2$  and  $\kappa_1$ :

$$\xi \equiv \rho(\kappa_2) - \rho(\kappa_1) \quad .\tag{7.2}$$

Note that we make  $\kappa_2$  the sublattice on which atoms lie preferentially as in Figure 2. Figure 5 shows how the long-range order,  $\xi$ , changes as a function of temperature. We chose the chemical potential as  $\mu/\epsilon = -40$ .

A typical calculation of  $kT/\epsilon = 4$  and  $\mu/\epsilon = -4$  was timed as follows. The CPU time used by the VAX/VMC computer was 200 minutes for 450 major iterations. The corresponding calculation was done in ten minutes using the CRAY computer of U.S. Air Force Weapons Laboratory.

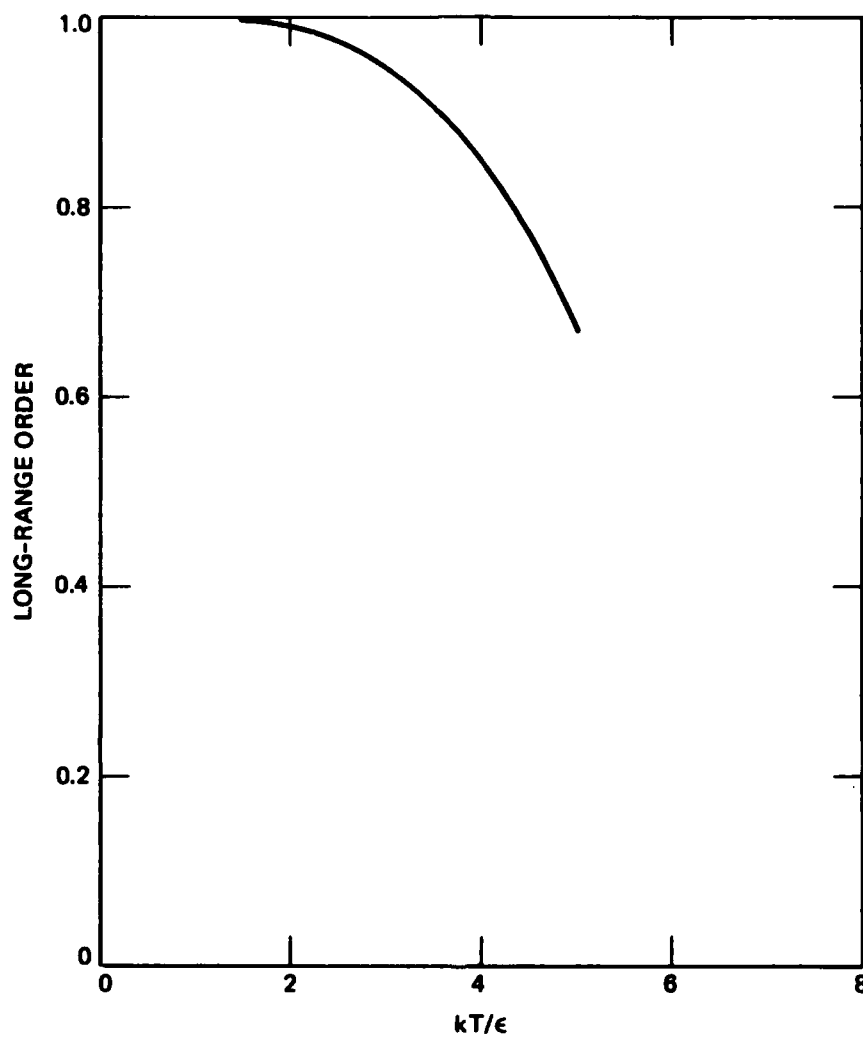


Figure 5. The long-range order parameter in the homogeneous bulk phase plotted against the temperature at  $\mu/\epsilon = -4.0$ .

### 8. Boundary Calculations

We use the results of the homogeneous phase calculations as the end condition of the boundary calculations. We choose

$$kT/\epsilon = 4 \quad \text{and} \quad \mu/\epsilon = -4, \quad (8.1)$$

which are for the long-range order of 0.85, as we see in Figure 5.

a. Width of the System. For the boundary computations we choose the lattice plane number,  $n$ , in Figure 2 to go from 1 through  $n_w$ , the center being at  $n_c = (n_w + 1)/2$ . If  $n_w$  is too small, the end effect of the system makes the calculated results unreliable. If  $n_w$  is too large, the memory space of the computer cannot contain all of the variables we need. As a compromise we chose

$$n_w = 17 \quad \text{and} \quad n_c = 9 \quad . \quad (8.2)$$

b. Left-Right Symmetry. In the actual computations, we do not need to work for  $n$  from 1 through  $n_w$ . Since the left- and right-hand sides of the system are symmetric, we can work for  $n$  from 1 through  $n_c + 1$  and use the left-right symmetry relations. We note the following kinds of symmetry:

$$V^3_{9-n, \kappa v; k+(1 \pm 1)6, j+(1 \pm 1)6, i+(1 \pm 1)6} = V^3_{9+n, \kappa; i+(1 \mp 1)6, j+(1 \mp 1)6, k+(1 \mp 1)6} \\ \text{for } i, j, k = 1, \dots, 6 \quad . \quad (8.3a)$$

These are for the left and right columns of Table 2. For the center column of Table 2, we have

$$V^3_{9-n, \kappa v; k'+6, j'+6, i'+6} = V^3_{9+n, \kappa; i+6, j+6, k+6} \quad . \quad (8.3b)$$

In these expressions,  $\kappa v$  is a function of  $\kappa$  and takes the value

$$\kappa v = 4, 5, 6, 1, 2, 3, 7, 8, 9 \quad , \quad (8.4)$$

corresponding to  $\kappa = 1, \dots, 9$ . The primes on  $i'$ , etc. in Equation (8.3b) are defined as

$$i' = i \quad ,$$

$$\text{except } i' = 2 \quad \text{when } i = 3 \quad ,$$

and

$$i' = 3 \quad \text{when } i = 2 \quad . \quad (8.5)$$

The symmetry relations for  $\alpha$ 's are

$$\alpha_{9-n, \kappa\alpha; j+(2-m)6, i+(2-m)6} = -\alpha_{9+n, \kappa; i+6m, j+6m} \quad (8.6a)$$

for  $i, j = 1, \dots, 6$  and  $m = 0, 1, 2$ .

The subscript,  $\kappa\alpha$ , is defined as

$$\kappa\alpha = 7, 8, 9, 4, 5, 6, 1, 2, 3, \quad (8.6b)$$

corresponding to  $\kappa = 1, \dots, 9$ . Note the minus sign on  $\alpha$  on the right-hand side of (8.6a).

The symmetry relations for  $\gamma$ 's are

$$\begin{aligned} \gamma_{LL}^{9-n, \kappa v; n, m, l} &= \gamma_{RR}^{9+n, \kappa; l, m, n} \\ \gamma_{RL}^{9-n, \kappa v; n, m, l} &= \gamma_{LR}^{9+n, \kappa; l, m, n}, \end{aligned} \quad (8.7)$$

where we use  $\kappa v$ , defined in Equation (8.4).

c. Initial Values. To start the iteration, the initial values of the V3 variables are chosen as follows. For  $n = 1, \dots, n_c - 1$ , V3's are set equal to the homogeneous phase values. At the center,  $n_c$ , we choose V3 as the average of the left-side homogeneous phase value and its symmetry value (calculated by the relations in Equation (8.3)). We use the same idea in choosing the initial values of  $\alpha$ 's and  $\gamma$ 's.

d. End Condition. After the iteration has started, we choose the end condition at  $n = 1$  and 2 so that the values of V3 at  $n = 1$  and 2 are the same.

e. Computer Time and Memory. When we choose  $n_c = 9$ , as in Equation (8.2), the number of variables are 58320 V3's, 9720  $\alpha$ 's, and 23040  $\gamma$ 's, giving a total of 91,080 variables. If we count 9720 V2's and 11,520 V3's instead of V3's, the total number of variables is 54,000. Using the CRAY computer, 150 major iterations were done in 50 minutes CPU time.



When we used the CRAY computer at AFWL, the case of  $n_c = 9$  was done, but the  $n_c = 15$  case was not, due to the lack of memory space. The VAX/VMS computer has a virtual memory system and could calculate the  $n_c = 15$  case.

f. Profile. The density profile of the boundary is shown in Figure 6. The  $\kappa$  numbers are those in Figure 2. The  $\kappa = 2$  point is the occupied lattice point in the homogeneous end-phases. The  $\kappa = 6$  and 7 points are the occupied points on the left end and the unoccupied points on the right end.

12263-16

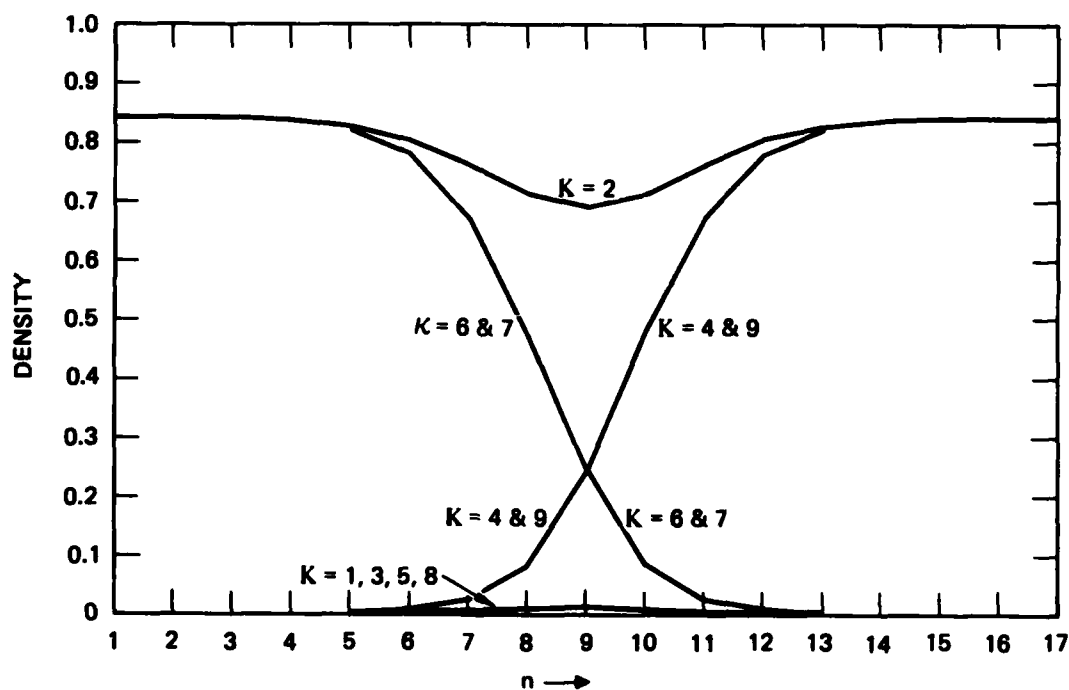


Figure 6. Density of atoms on each sublattice, at  $kT/\epsilon = 4$  and  $\mu/\epsilon = -4$ . The density of the homogeneous phase is 0.843.

## 9. Conclusion

A model of a three-dimensional grain boundary has been calculated using statistical mechanics for the first time.

The cluster variation method (CVM) is capable of treating such a three-dimensional problem. A set of simultaneous equations of a large number of variables (54,000 variables or 91,080 variables, depending on how they are counted) can be solved using the natural iteration method (NIM).

The CRAY computer can calculate the boundary about ten or more times faster in CPU time than the VAX/VMS computer.

#### REFERENCES

1. R. Kikuchi, J. Chem. Phys. 66, 3352 (1977).
2. R. Kikuchi, J. Chem. Phys. 68, 119 (1978).
3. R. Kikuchi and J.W. Cahn, Acta Met. 27, 1337 (1979).
4. R. Kikuchi and J.W. Cahn, Phys. Rev. B21, 1893 (1980).
5. R. Kikuchi, J. de Phys. 38, C7, 307 (1977).
6. P.J. Goodhew, T.Y. Tan and R.W. Balluffi, Acta Met. 26, 557 (1978).
7. M. Kurata, R. Kikuchi, and T. Watari, J. Chem. Phys. 21, 434 (1953).
8. R. Kikuchi, J. Chem. Phys. 65, 4545 (1976).

APPENDIX C

TRANSITIONS AND PHASE EQUILIBRIA AMONG GRAIN BOUNDARY STRUCTURES

John W. Cahn  
Center for Materials Science  
National Bureau of Standards  
Washington, DC 20234

PRELIMINARY VERSION

Subject to Review at National Bureau of Standards

DO NOT QUOTE WITHOUT PERMISSION.

**Abstract** - The characteristics of equilibrium first-order phase changes of the grain boundaries themselves are such that it leads to a definition of grain boundary phases in which smoothly curving boundaries are of the same phase. Different grain boundary phases coexist at facet edges and corners. The phase rule, phase diagrams, and some phase change mechanisms are developed. For a wide variety of problems orientation of the normal is shown to be analogous to composition in ordinary three-component systems. The role of symmetry in modifying the phase rule and in sectioning phase diagrams is explored. Reports of boundary phase changes are re-examined critically.

**Introduction** - Transformations of grain boundary structures have been invoked to explain observations of discontinuities of grain boundary properties as temperature, composition and even thermal history are varied [1-9]. This explanation has led to the concept of grain boundary phase transformations which assumes that grain boundaries are two-dimensional phases, that there can be several distinct such phases each having a free energy, and that there will be a phase change whenever these free energy curves cross. At such transitions, properties can change discontinuously but, as has been pointed out, there are limits [2,10,11]. The boundary free energy can't be discontinuous as has been reported [3].

Phase changes of single crystal surfaces are well documented [12-13]. Careful studies on planar surfaces reveal their two dimensional space group symmetry. Discontinuities in properties, such as adsorption, have not only been documented, but symmetry changes, which necessarily mark a phase change that could be higher order, occur frequently.

Grain boundaries have rarely been studied with such care. Even the best studies have dealt with curved boundaries and since properties of boundaries, including their symmetry, depend on orientation, the question of what is a grain boundary phase needs to be answered before we can ask if there has been a change of phase.

In this paper we defer this question. We assume that there are indeed several stable or metastable structures of a grain boundary for each orientation. We compare these to find the most stable structure or combination of structures. From this comes the surprising result that only a few specific orientations can transform congruently, i.e. without a change of shape. Almost all grain boundary phase transitions involves faceting to different orientations. As a consequence, a natural definition of grain boundary phases and coexisting phases at equilibrium presents itself. The several types of phase transitions then are re-examined. We include wetting transition in which a phase not stable in bulk forms along a grain boundary but we exclude the bulk phase changes that originate at grain boundary.

We begin by specifying the state variables of grain boundaries, examine conditions for equilibrium and then develop the properties of diagrams of state or phase diagrams.

**Grain Boundary State Variables** - As with three-dimensional phases, there are a number of variables that define the state of a planar grain boundary. The structure and properties of an equilibrated boundary are fully specified when these variables are fixed. Because the boundary is free to exchange matter and energy with the grains, it acts as an open system. As a result, temperature and chemical potential are the natural thermodynamic variables for describing the reservoir. Gibbs' proof [14] that temperature and chemical potential are constant throughout a system of surfaces and phases is readily extended to include grain boundaries [2,14,15]. Since grain boundary temperature and chemical potentials are specified by temperature, pressure, and composition of a grain, these could equally well serve as state variables of the grain boundary. With this latter set the grain boundary

remains an open system as long as the grain size is large enough that changes in adsorption will not affect the grain composition. The alternate choice of a compositional state variable, the level of adsorption, has many disadvantages. It is not as easily measured and in an equilibrated polycrystalline specimen varies from place to place on the boundaries.

In addition to these standard thermodynamic variables, the state of the boundary depends on geometric variables. Three angular variables specify  $R$ , the misorientation between the two abutting grains. Two angular variables specify  $N$ , the orientation of the grain boundary normal. There are four more translational variables [16] that we will ignore because they are usually, but not always, allowed to relax to equilibrium. In some experiments the angular variables are also allowed to relax to equilibrium [17]. Grains can rotate and boundaries can facet to other orientations. We will specifically assume that  $R$  and the average of  $N$  are specified.

The total number of grain boundary state variables is therefore six plus the number of chemical components. There are five angular variables ( $R$  and  $N$ ), temperature, and either one chemical potential for each of the components or pressure and the composition. Area is the extensive variable. We will mostly specify area projected along  $N$ . This is the area that is fixed if we specify a planar curve to be the perimeter of the boundary. The boundary then is able to find a minimum free energy at the fixed projected area even if that minimum includes faceting or zigzagging to orientations of lower energy [18].

Grain Boundary Equilibrium - The appropriate free energy is one that is minimized at equilibrium under the conditions specified by the method of the observation. We fix the perimeter of the grain boundary to be a plane curve and permit matter and energy to be exchanged with the abutting grains of fixed temperature and either fix chemical potentials or composition and pressure. For grain boundary, as well as surface equilibrium, it is the excess in  $E - TS - \sum \mu_i N_i$  per unit area projected along  $N$  that is to be a minimum [15,18,19]. This excess free energy per unit area has been variously described by the symbols  $\sigma$  or  $\gamma$ . We use  $\gamma$ .

Equilibration of a grain boundary involves reducing  $\gamma$  to its lowest value. This may involve exchanges of energy and matter with the grains, structural rearrangement, and faceting. For the purposes of this paper we consider not just the lowest value of  $\gamma$  but several grain boundary structures that are in metastable or unstable equilibrium. These other boundaries are at stationary values of  $\gamma$  that are local minima.

Such other structures are a familiar concept in metastability. They provide a vehicle for the description of first order phase changes in which quite different structures become the stable phase as the state variables are varied and give rise to a phase diagram whose dimension equals the number of state variables, which maps the bounds to the stability of a grain boundary phase.

First Order Grain Boundary Phase Transformations - The simplest way to examine grain boundary phase transformations is to image two or more different grain boundary structures and to examine graphically how their  $\gamma$  values vary with one of the nongeometric state variables. Thermodynamics requires that for these variables each of the  $\gamma$  plots be continuous. Let us examine a range of temperature over which two such hypothetical  $\gamma$  curves cross. For two forms of a fluid surface in a one component constant pressure system, there would be a phase change between these two forms exactly where the two curves cross. This situation is identical to a first-order one-component phase change in three dimensions with Gibbs energy instead of  $\gamma$  as the ordinate.

To demonstrate that this simple example is misleading for solid boundaries, we turn to a familiar problem in another field. It is well known that phase changes in a system with fixed average composition do not usually occur simply at the place where the molar Gibbs free energies of the phases cross [20-22]. Figure 1 shows a

pair of intersecting isothermal constant pressure free energy curves in a binary system. The common tangent represents a two-phase equilibrium of coexisting phases, differing in composition, at a lower free energy than either curve in that composition range. The loci of intersections of free energy curves in such a system do not mark phase changes. Because only the average composition is specified, the system is free to seek equilibrium with a lower free energy in a combination of phases of differing compositions. This is the essential distinction between the constructions in the one and two component systems: both phases must have the same temperature, while only the average composition is specified.

Equilibrium is expressed by a convexity theorem, which requires that the isothermal molar free energy vs. composition curve be convex as seen from below. This convex curve, consisting of segments of curves and tangent lines, is depicted in Figure 1. The curved portions represent single phases, the tangent lines represent the free energies of mixtures of phases whose compositions are those of the contacts. This construction eliminates not only any concave bulges but also the intersections of free energy curves. As temperature and pressure change the free energy curves, the compositions of the two-phase region shifts. These shifts are graphically represented on phase diagrams. Of special interest are conditions where two free energy composition curves touch without crossing. These represent congruent phase changes, where two phases of the same composition are in equilibrium.

In multicomponent systems the free energy-composition plot at constant temperature and pressure is a hypersurface. Equilibrium requires that this hypersurface also be convex and that concave bulges be eliminated by hyperplanes. The phase rule [14,20,21] is an expression of how many phases can coexist and has a very simple geometrical interpretation in terms of these tangents. It must be amended when symmetry is present, as in mixtures of isotopes or enantiomorphs [23]. Symmetry of the free energy hypersurface can permit more simultaneous tangent contacts.

An important aspect of phase diagrams concerns which of two kinds of variables are chosen as axes [24]. Quantities such as composition need not be the same in coexisting phases. Hence, they lead to gaps in compositions that are multiphase regions and to tie lines, tie triangles, etc., across these gaps to indicate the composition of coexisting phases. Quantities such as temperature, pressure, and chemical potentials have the same value in all coexisting phases. If they are axes on a phase diagram, the tie lines must be perpendicular to these axes. If all axes are of this type no gaps can occur. Multidimensional phase diagrams sectioned perpendicular to such axes are easier to interpret because coexisting phases always lie within such a section.

We now imagine two different grain boundary phases that are represented by two intersecting  $\gamma$  curves. For the present each curve is assumed to be a continuous function of all the state variables including  $N$ . Does the locus of points of intersection mark the condition of phase transition? Because of the open system conditions, the temperature and chemical potentials of all coexisting grain boundary phases are the same. Thus we must compare grain boundary phases at the same temperature and chemical potentials. This is true even if we use grain compositions as our variables. The geometric variables require special examination. We may try to impose a misorientation  $R$ , but grain boundaries are known [25] to dissociate into several grain boundaries whose combined misorientations are equivalent to  $R$ . The orientation  $N$  has the character that only its average is usually specified but the boundary is free to facet or zigzag.

There are several constructions that are useful for examining the  $N$  dependence. Herring [18] derived a tangent sphere construction for examining stability which Frank [26] simplified by inverting  $\gamma$  in which the test sphere became a tangent plane. This was then used by Hoffman and Cahn [19,27] to construct  $\xi$  a vector function of  $\gamma$ . Both of the last two lend themselves readily to examining the  $N$  dependence.

Frank took the reciprocal of  $\gamma$  and showed that a plot of  $\gamma^{-1}$  in polar coordinates

had to be convex; i.e., any tangent plane to  $\gamma^{-1}$  had to stay outside the  $\gamma^{-1}$  plot. Inward bulges were to be filled in with tangent planes representing hill and valley structures (Fig. 1). The geometrical convexity condition for this three-dimensional surface is mathematically identical to the condition encountered in three-component phase equilibria. The behavior of  $N$  in surface and grain boundary phase transitions is identical to the behavior of two compositional variables in a three-component system.

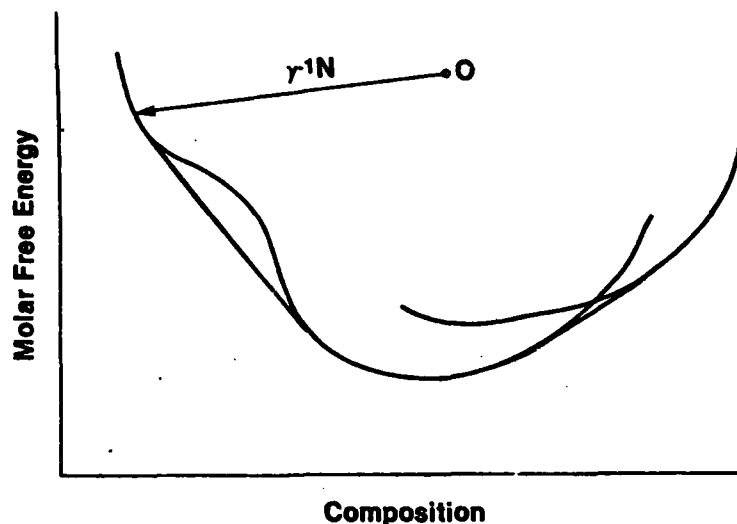


Fig. 1 : The same tangent construction is used for the coexistence of phases, using a cartesian plot of molar free energy vs. composition, and of facets, using a polar plot of  $\gamma^{-1}(N)$ . The tangent eliminates all concave portions, whether caused by a bulge in a single curve or by intersecting convex curves.

The development of the  $\xi$  vector leads to identical conclusions. The  $\xi$  vector is constructed from  $\gamma$  [19,27]. The loci of  $\xi$  vectors forms a surface whose inner envelope is a closed convex surface whose shape is that of a grain of fixed volume embedded within another, misoriented by  $R$ , with minimum total grain boundary free energy. The  $\xi$ -plot represents the actual orientations present. Orientations that are unstable with respect to faceting are absent, and graphically seen as corners and edges. The edges of any  $\xi$  plot mark two coexisting orientations; corners mark coexistence of more than two orientations. If there were two kinds of grain boundary structures with intersecting  $\gamma$ , there would be two intersecting  $\xi$  plots (Fig. 2), whose inner envelope would necessarily have a sharp edge indicating that certain orientations would always be absent at equilibrium. The coexisting phases would meet at an edge in the  $\xi$ -plot. They would display an edge with the same orientations in a real specimen at equilibrium.

Convex portions of  $\xi$ -plots outside the inner envelope are metastable, and facet by nucleation of patches of a new orientation. Portions that are not convex are unstable with respect to continuous reorientation. Concave bulges in Figure 1 lead to self intersections in Figure 2 with convex and concave portions separated by spinodals [27-29].

Except for congruent phase changes, and the unlikely possibility that  $\gamma$  is not a function of  $N$ , all equilibrium phase changes involve the formation, elimination, or other changes in edges and corners of a grain boundary. Equilibria between these different structures would almost always occur as observed edges and corners in a hill and valley structure. Facetting can also occur if we assume a single  $\gamma$  curve with a concave bulge. Such free energy bulges are analogous to those encountered in miscibility gap systems that have critical points. The coexisting phases are different phases. At such critical points the phases become identical. The analogy holds for grain boundary phases.



We now propose to define grain boundary phases such that all equilibrium edges and corners represent coexisting phases. This includes all coexistence based on the assumption of several metastable structures with the same  $N$ . In this definition curved grain boundary without singularities in its shape is all of the same phase. The structure of this grain boundary phase varies as the orientation changes, just as the structure of a chemical phase varies over its composition range. Phases differing by a first-order phase change coexist at edges and corners (except when it is a congruent phase change). Singularities in shape other than discontinuities in orientation represent higher order phase changes.

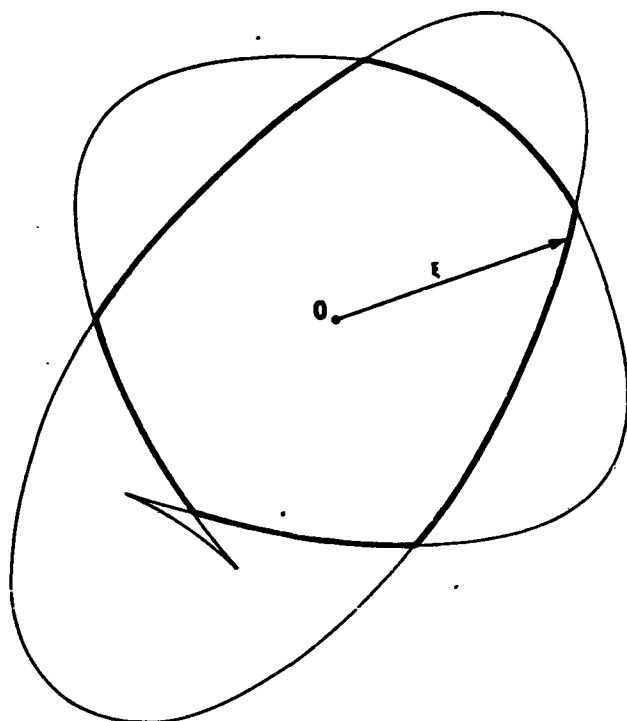


Fig. 2 : The inner envelope of a  $\xi$  plot shows the actual orientations of stable boundaries. Orientation discontinuities (edges) represent coexisting orientations (facets). Intersecting  $\xi$  plots necessarily lead to orientation discontinuities. Self intersecting portions of the  $\xi$  plot result from bulges in  $\gamma^{-1}$  plots, and show "ears" with inelastable convex portions and unstable concave portions separated by spinodals.

Sometimes the coexisting grain boundary phases have identical properties by symmetry. This, too, has an analogy in three-dimensional phase diagrams. Systems with enantiomorphs have different phases that are mirror images of each other with identical properties. As in the case of enantiomorphs, symmetry leads to modifications of the phase rule for grain boundary phases [23].

We began by assuming the existence of two different structures with two different  $\gamma$  curves and concluded that, except for the congruent orientation where two different planar boundaries transform into each other, most phase changes involve the formation of patches of grain boundary with different orientations. We also began by assuming that  $\gamma$  was a continuous function of  $N$ . This, too, is not essential. Frank's  $\gamma^{-1}$  and our  $\xi$  plot are continuous convex figures even if  $\gamma$  is not. Planes or ruled surfaces alternate with doubly curved portions. In the polyhedra as the curved portion have shrunk to points on the  $\gamma^{-1}$  plot and have become the planes on the  $\xi$  plot.

The convex  $\gamma^{-1}$  plots are continuous functions of  $N$ . The Gibbs adsorption equation insures that  $\gamma$  is a continuous function of  $R$  and the chemical potentials. Stability consideration requires that  $\gamma$  either be continuous in  $R$  or dissociate into boundaries whose combined  $\gamma$  is continuous in  $R$ . Thus  $\gamma$  is continuous through phase transitions whether the transition is congruent or proceeds by facetting, or which of the state variables is varied. Reports that  $\gamma$  be discontinuous is contrary to thermodynamic stability principles. It cannot be explained by any artifact such as impurities [3,5] which, after all, are just chemical components.

Many correlations follow from this rigorous mathematical analogy between orientation of surfaces and composition in a three component system. These will be developed in the next section as part of an examination of all the state variables and the full phase diagram.

Grain Boundary Phase Diagrams - We next examine a space of all  $6+C$  state variables, where  $C$  is the number of chemical components. Five axes are angular variables, three to specify  $R$  and two to specify  $N$ . These specify temperature the chemical potentials or activities of the components. Each point in this hyperspace represents a state of a grain boundary. Some regions represent stable planar boundaries of a particular phase, other regions represent the fact that a boundary with these state variables is decomposed into segments of several boundaries, each segment being of a different phase.

The examination of this hyperspace is greatly simplified by the realization that any set of coexisting grain boundary phases share the same temperature and chemical potentials. Hence grain boundary phase diagrams can be sectioned at constant temperature and chemical potentials with the knowledge that all tie lines (or tie figures of higher connectivity), connecting points that represent the coexisting boundary phases, lie entirely within that section. This section still has the five dimensions of the  $R$  and  $N$  axes, but the  $6+C$  dimensional diagram can now be thought of as an evolution of five-dimensional diagrams as  $T$  and the chemical potentials are varied.

The five-dimensional diagram can be sectioned further. If all facets have the same misorientation  $R$  across them, then all tie figures lie within a constant  $R$  section. This is a two-dimensional section with  $N$  as its axes. Such  $N$  diagrams have the features of an isothermal constant-pressure section of a ternary phase diagram plotted onto the surface of a unit sphere instead of an equilateral triangle.

Although  $R$  can be imposed by creating a bicrystal with that misorientation, the system will dissociate this boundary into several with a combined  $R$  equal to the original misorientation if that will lower the energy. One such dissociation has been demonstrated [25]. When a high energy boundary has the combined misorientation of two known low energy boundaries, such as twins or special coincidence site boundaries, such boundaries dissociate. The resultant coexistent boundaries have  $R$  values different from the imposed  $R$  and therefore do not lie in a constant  $R$  section. The twin part of the dissociated boundary has been observed to facet [25]. In this case the tie lines cannot be counted on to be perpendicular to any axis. Unless there are some special symmetries, the representation of the phase coexistence requires the full five-dimensional space.

The construction rules for coexistence of dissociated boundaries differs from that of the usual phase diagram. The combined  $R$  is conserved in a dissociation, whereas the average  $N$  or composition is conserved in facetting or phase separation. As a result, the limits of regions that represent undissociated boundaries do not represent  $R$  values of the components of a dissociated boundary. No method of representing dissociations on the diagram has been suggested.

The sections of the  $C+6$  dimensional phase diagram parallel to temperature or chemical potential axes may have tie lines at an angle to the section. This is a familiar complication in "vertical" sections of ternary phase diagrams in which temperature or pressure are the vertical axis. If there is no dissociation, such sections should look quite similar to such vertical sections.

Vertical sections containing all tie lines exist for ternaries. These sections are true binaries. They are sometimes called quasibinaries. Symmetry is an important guide for finding such vertical sections for grain boundaries. (Vertical sections of surface phase diagrams have been given [12,13] for symmetric orientations.)

The Phase Rule - Many years ago, Defay [31,32] proposed a surface and interface phase rule for systems with several bulk fluid phases and allowed for possibility of a multitude of interfaces between pairs of different phases. He dealt only with the usual  $C+2$  state variables. His phase rule should not be applied to solids because it does not take into account the multitude of solid phenomena, e.g., orientation effects. What we develop here is a localized grain boundary phase rule for a single phase polycrystalline solid. It deals with how many grain boundary phases can coexist at a point on a grain boundary and whether this coexistence remains if we change the state variables. The rule is easily modified if there are several bulk phases but it remains a local phase rule. The phase rule is a useful concept for phase diagrams of first order transitions. The derivation of a phase rule assumes that all grain boundary phases have different fundamental equations for how  $\gamma$  depends on the state variables. This is frequently not the case. When high symmetry grain boundaries facet, they will facet into symmetry related orientations, and the phase rule must be amended for symmetry. Fortunately the  $\gamma^{-1}$  and  $\xi$  constructions are geometrical constructions completely consistent with the phase rule and, as will be shown, these permit us to specify what happens at the exceptions.

When all grain boundary phases are different, the phase rule specifies that the degrees of freedom  $F$  is given by

$$F = C - P + 7 \quad (1)$$

where  $C$  is the number of chemical components, and  $P$  the number of grain boundary phases all nonequivalent. When there is more than one bulk phase the phase rule becomes

$$F = C - (P + P_B) + 8 \quad (2)$$

where  $P_B$  is the number of bulk phases.

If  $R$ ,  $T$ , and the chemical potentials are specified (or equivalently pressure and the composition), we obtain the rule for an  $N$  diagram, again for nonequivalent phases.

$$F = 3 - P \quad (3)$$

which is the same as for a three-component phase diagram at constant  $T$  and pressure. We examine these  $N$  diagrams with special emphasis on the symmetry effects. Because crystal surfaces share all the same state variables with grain boundaries except  $R$ , the properties of this section apply equally to surfaces. We have given a more complete treatment for surfaces.

The  $N$  Diagram - In order to examine the properties of an  $N$  diagram, we assume that all tie lines lie within that section.  $R$  is assumed fixed and stable with respect to dissociation. We then know a great deal about the properties of such a section for it is equivalent to a isothermal constant pressure section of a three-component phase diagram plotted on the surface of the unit sphere instead of an equivalent composition triangle.

We first examine phase coexistence when all phases are nonequivalent. In an  $N$  diagram, because  $R$ ,  $T$ , and the chemical potentials are specified, equation (3) applies. Single-phase regions have the two degrees of freedom that permit  $N$  to range. Smoothly curved boundaries in an experiment plots are single phases. So are smoothly curved regions of a  $\xi$  plot, as are those curved convex regions on a  $\gamma^{-1}$  plot. The single phase on the  $N$  diagram can occupy the entire unit sphere, or it can be bounded by phase changes. Two-phase coexistence is represented by two curves ( $F = 1$ ) connected by tie lines representing coexisting orientations. The space on the diagram between the curves are forbidden orientations, edges in an experiment and on a  $\xi$ -plot. The tie lines and coexistent phases are formed by a rolling tangent plane on the  $\gamma^{-1}$  plot. Tie lines are

great circle segments, whose poles are directions of the tangents to the edges they represent.

These two-phase regions may form smooth closed curves. They may also terminate at critical point where the two phases have become identical or at three phase coexistence. On a  $\xi$ -plot critical points are end points of edges in which the crease terminates and is smooth thereafter. It is represented by a terminating orientation gap on an N diagram. Three-phase coexistence is a corner in the experiment or on a  $\xi$ -plot, a tangent contacting the  $\gamma^{-1}$  plot at three points. It is represented by a tie triangle on the N-diagram.

To obtain congruent points or "more than three-phase" coexistence, one or more of the other state variables must be changed, or symmetry has to be present.

Both  $\gamma$  as a function of N and the N-diagram must obey the Wulff group point symmetry W imposed by R [33]. For surfaces this point symmetry is that of the crystal. For grain boundaries, it is derived [16,34,35] from the point symmetry of the grains and R. The set W of resulting point groups include the usual 32 point groups plus 14 additional with 8 and 12 fold axes, a total of 46. We call these latter point groups octagonal and dodecanogal.

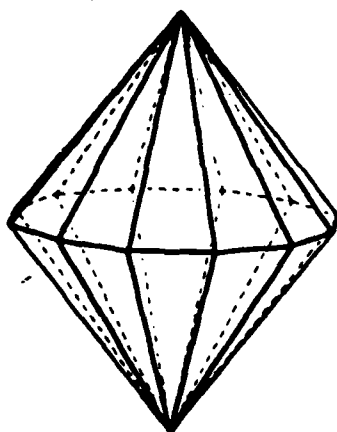
The effect of symmetry is most easily seen using the  $\xi$ -plots. Nothing is changed for single and two-phase coexistence, which are still represented by surfaces and curved edges. Only two surfaces can meet at an edge of a convex inner envelope. More than three surfaces can meet at corners. We may use crystallographic form theory [36] to specify how many.

For the 32 classical point groups, there are 47 forms resulting from intersections of planes that are equivalent by symmetry. Many are prisms and pinacoids composed of planes parallel to an axis, that do not form corners. The remainder have corners where three or more equivalent planes meet. Corners also result from combined forms in which planes that are not all equivalent intersect at a point. There are additional forms that originate in the octagonal and dodecagonal point groups.

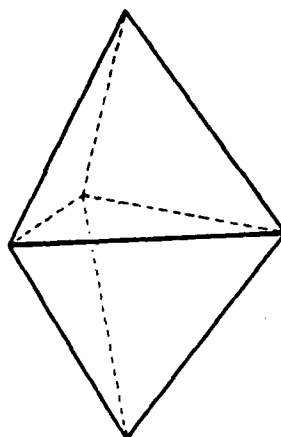
There are two classes of forms. There is one general form, in which the planes have general indexes, for each of the 46 point groups except 1. There are in addition special forms for special Miller indexes.

We examine all the forms for corners. Table I gives the number of facets along the axis for tetragonal, hexagonal, octagonal and dodecagonal forms for general indexes and the two kinds of special indexes that do not give pinacoids or prisms. This number is equal to the number of coexisting facets if the basal plane facets. Figure 3 shows the dihexagonal dipyrmaid and the trigonal dipyrmaid. These are general forms in the hexagonal ( $r = 6$ ) system for  $6/mmm$  and  $\bar{6}$  respectively show 12 and 3 sided corners. If the basal plane were to facet into planes with general indexes, there would be 12 and 3 facets if the Wulff group were  $6/mmm$  or  $\bar{6}$  respectively. It is interesting to note that the number of faces either remains the same or decreases if faceting occurs at a special orientation. The indexes of the facets, of course, refer to those of the dichromatic pattern or the two interpenetrated crystals and not to those of either crystal.

Table II gives the number of facets in the cubic system if either the cube plane or the octahedral plane facets. The numbers divisible for 3 are those for the octahedral plane. Whenever there are parenthesis around them (111) and  $(\bar{1}\bar{1}\bar{1})$  give different answers. In contrast to Table I, the number of facets is often larger for special orientations. All faceting of basal planes in the trigonal system yields 3, except for  $hkil$  and  $hh2h1$  in point groups 32 and  $\bar{3}m$  which yield 6. Four-sided corners occur along the 2-fold axis in  $mm2$  and along all three axes in  $mmm$  for special indexes only. All other four-sided corners arise from mirror planes or combined forms.



Dihexagonal dipyrmaid



Trigonal dipyrmaid

Fig. 3 : Forms of  $\xi$  plots must conform to the symmetry of the Wulff group. The basal plane will facet into 3 and 12 orientations for 6 and  $6/mmm$  respectively. Note also the meeting of four orientations at the mirror plane in  $6/mmm$ .

Table 1. The number of equivalent facets replacing the basal plane, listed by point group and facet indexes when the rotation axes are  $r$ -fold with  $r = 4, 6, 8$ , and 12.

Point Group	Facet Index		
	$hkl$ $hk11$	$hh1$ $hoh1$	$h01$ $hh2h1$
$\frac{r}{r}$	$r$	$r$	$r$
$r/m$	$r/2$	$r/2$	$r/2$
$r22$	$r$	$r$	$r$
$rmr$	$2r$	$r$	$r$
$\overline{r}m2$	$r$	$r/2$	$r$
$r/mmm$	$2r$	$r$	$r$

Table II. The number of equivalent facets replacing the cube and octahedral planes for cubic systems.

Point Group	Facet Index						
	$hkl$	$hh1$		$hk0$	$111$	$110$	$100$
23	2,3	4,3	2,(3,6)	2,3	2,(3)	4,3	3
$m3$	4,3	8,3	4,3	2,3	4	4,3	3
432	4,3	8,3	4,3	4,6	4	4,3	3
43m	4,6	4,3	2,(3,6)	4,6	2,(3)	4,3	3
$m3m$	8,6	8,3	4,3	4,6	4	4,3	3

Four-sided corners arise along mirror planes whenever an edge intersects a mirror plane. This can be seen along the basal plane of the dihexagonal dipyrmaid. It also occurs in combined forms in systems with symmetry as low as  $m$  (Fig. 4).

Although these multiphase equilibria range from  $P = 3$  to  $P = 24$  they occur in  $N$  diagrams without requiring more degrees of freedom than for  $P = 3$ . If a tangent plane contacts the  $\gamma^{-1}$  surface at three equivalent points, it contacts all points that are equivalent by symmetry. If a tangent plane contacts two points on one side of a mirror, it can contact either none or two points on the other side.

If we use the other degrees of freedom to adjust the relative  $\gamma$  values of different phases, we can achieve multiple contacts in combined forms. Each additional form requires a degree of freedom, just as it does when all phases are different in equation 1. No more than three facet orientations are ever needed to reach a minimum free energy [37] for an undissociated boundary, or for each component boundary in a dissociated one. When the phase rule permits more facets, many degenerate structures are possible.

For the purpose of the phase rule, two phases related by symmetry count as two phases, while three or more count as three phases.  $M$  pairs of phases related by a mirror plane count as  $M+1$  phases.

The Search for Congruent Transformations - Congruent phase changes do not, in general, occur in a constant  $R$ ,  $T$  and chemical potential section. This can be easily seen from the phase rule and from the  $\gamma^{-1}$  or  $\xi$  plots. Congruent points occur on these plots only when the  $\gamma^{-1}$  or  $\xi$  plots of one phase contacts the other at a point without intersecting. We therefore need to adjust one of the other state variables to obtain precisely this condition. The search for congruent transformations has all the aspects of a search for a needle in a  $6+C$  dimensional haystack. Nonetheless one congruent phase transformation has been found experimentally and theoretically, making use of known symmetries. Congruent phase changes are likely to occur at high symmetry orientations because  $\gamma$  has an extremum there and the tangent contact requires the same slope for both phase. But there seems to be no increase in the degrees of freedom because of symmetry for this transition.

Glicksman and Vold [38] found a congruent grain boundary melting transition in bismuth, as the varied  $R$ . The rotation axis was the trigonal 3 axis. For a general rotation the dichromatic pattern symmetry is  $3m'$  with the colored mirror planes bisecting directions in the two crystals related by the rotation. The Wulff group symmetry for  $\gamma$  is thus  $3m$ . The symmetric tilt boundaries studied lie along these mirror planes. Mirror planes by themselves do not guarantee a symmetry dictated extremum, but in a  $3m$  the mirrors are part of a  $2/m$  axis that is sufficient. These boundaries are likely candidates for congruent transformations as  $R$  is varied. The nonsymmetric boundaries that do not lie along the mirror planes facet on cooling through the melting transition [39].

A congruent melting transition was also found theoretically [40] by varying  $T$  for a symmetric  $\Sigma = 5$  boundary in a two-dimensional square lattice gas crystal. Again the required symmetry was present.

Neither of these studies provided clean examples of how  $\gamma$  should vary through a first order congruent transition i.e. that  $\gamma$  be continuous but with a discontinuity in slope. In the bismuth experiments, the grain boundaries were equilibrated with solid-melt interfaces whose  $\gamma$  was measured and shown to be almost isotropic. The dihedral angle of the grain boundary groove changed discontinuously at the melting transition.

One-dimensional features do not show clean phase transitions, only regions of rapid change. The grain boundary between two two-dimensional crystals is such a one dimensional feature, and the calculated phase transition had the expected gradual nature [40].

The Controversy About Dihedral Angle Discontinuities - In 1970 Gleiter [3] examined a trijunction in lead and reported a discontinuity in the dihedral angles as temperature was changed. Glicksman and Vold [38] reported a discontinuity in the grain boundary melt groove angle as  $R$  is varied. Both sets of investigators adopted a common fallacy that interprets dihedral angles in terms of ratios of  $\gamma$ 's and ignores the torque terms that result from the  $N$  dependence of  $\gamma$ . Since thermodynamics requires  $\gamma$  to be continuous at phase transitions no discontinuity in the ratio of  $\gamma$ 's is possible. As a result, Gleiter's interpretation has been repeatedly criticized [2,10,11].

Much of the discussion has centered on the role of hypothetical impurities. But impurities are chemical components, and if the system is equilibrated should not affect the continuity of  $\gamma$ . Gleiter's claim that the angular discontinuity was reversible is evidence for equilibrium.

A close comparison of Gleiter's Figures 4a and 4b [3] reveal evidence for the onset of facets at the transition. Coexistence of facets is not only evidence of phase coexistence, but it is also evidence of torque terms resulting from the  $N$  dependence of  $\gamma$ . As can be readily seen from  $\xi$  vector constructions, there is no violation of thermodynamic principles by a report of a discontinuous change in two of the dihedral angles when one of the boundaries at a trijunction undergoes a facetting transition.

General Dissociation Transitions - The replacement of one grain boundary with several, whose combined misorientation has the imposed  $R$ , and whose combined  $\gamma$ 's is lower, is a special case of a more general dissociation phenomenon. When the grain boundary dissociates into two, a grain of the same phase has formed a layer that "wets" the original grain boundary, lowering its energy. When the bismuth grain melts it is replaced by two interfaces plus a layer of a different phase which wets the grain boundary. When a single layer wets the boundary it is easy to understand the phenomenon in terms of thin layers of three-dimensional phases bounded by two interfaces or grain boundaries [41,42]. Often the layer is not a homogeneous phase, but one that changes continuously. It then becomes easier to consider the boundary a region of continuous transition [43]. In this section we consider only the dissociation through the means of a wetting layer composed of a uniform phase and two interfaces or boundaries.

If the wetting layer is a different three-dimensional phase, we expect a wetting transition only if the thermodynamic cost of inserting this phase is negative. The phase is therefore likely to be one that is not too far from being stable in bulk. Since grain boundaries can not exist without the grains, the ultimate grain boundary phase transition occurs when the grains themselves change phase. At such a phase transition some grain boundaries will be wet and the thickness of the wetting layer is without limit. If conditions are changed so that the wetting phase is slightly unstable in bulk, it will remain at these boundaries but its thickness will be governed by forces between the two interface boundaries. Eventually as the wetting phase becomes more unstable, it may disappear from the grain boundary in a phase transition. Grain boundary melting transitions have been calculated to occur hundreds of degrees before melting.

In addition there is a singularity at the melting point itself. Because a wetting layer can increase without limit at the bulk phase transition, use of the Gibbs adsorption equation indicates that the temperature and chemical potential coefficients of  $\gamma$  must diverge. This too has been confirmed in a grain boundary melting calculation [40]. Wetting transitions are not confined to melting and dissociation. Solid state phase changes can also lead to wetting layers of a different solid phase. Surprising results [44] on grain boundary diffusion in iron might be an indication that this occurs.

Wetting occurs universally near critical consolution points because  $\gamma$  of the interface between the two critical phases is extraordinarily low [42]. As a result since the grain boundaries of one of the critical phases will have a lower  $\gamma$ ,

grain boundaries of the other critical phase will be wet. As two-phase coexistence is approached there could be two singularities; first either an abrupt transition to a wetting layer or a discontinuous change in adsorption, followed by the singularity when the other critical phase becomes stable in bulk.

Discussion - We have made an exact analogy between the orientation of a grain boundary normal and composition in a three-component system. They are similarly constrained by experiment. Only their averages are fixed and the system is free to lower its free energy by facetting or forming phases with different compositions. The same convexity rules and tangent construction hold for equilibria. Phase diagrams are similar, differing mainly in phase rule modifications because of symmetry.

These considerations led to an obvious definition of what we should call a grain boundary phase. A smoothly curved grain boundary is like an inhomogeneous phase. Phase coexistence occurs usually with discontinuities in orientation.

With 6+C state variables for grain boundary properties, symmetry has an important role in bringing the observations into a manageable form. It also plays a role in helping locate interesting features in phase diagram, in sectioning the hyperspace and in predicting deviations from the phase rule.

Consistent with the ternary analogy, phase transitions generally occur by the appearance of new orientations. The onset of facetting is a common observation. Often it is brought on by the addition of certain chemical components [45]. This must be interpreted as a phase change.

Dissociation and wetting are also commonly observed. The onset of wetting is seen as a phase transition as the state variables are varied. It has been found as  $R$  is varied [25,38] increasing  $\gamma$  of the boundary or as  $T$  is varied [40,41] changing the stability of the wetting phase. The transition from dissociated to undissociated boundaries has not been pinpointed.

Most of the previous discussions of grain boundary phase transitions have implicitly assumed congruent phase changes. We have found that this is a rare occurrence at equilibrium. Far from equilibrium it can occur, just as partitionless phase changes occur in the alloy analogue. Most of the expected observations in these discussions required a pinpointing of singularities in equilibrium properties and this requires observations near the equilibrium transition. None of these methods of observation are both easy and convincing. By comparison facetting is easy to observe, and so closely associated with grain boundary phase transitions, that we have chosen to define phase coexistence in terms of facets. The analogue to nucleation and growth and to spinodal decomposition has been made [29] in a paper that recognized the equivalence of orientation in problems of facetting mechanism with those of composition in phase changes.

Phase transitions far from equilibrium may proceed with a change of morphology. If, however, a transition is reported to occur congruently it is imperative that the transition be re-examined close to equilibrium. The observation may simply have been a relaxation back to equilibrium of a boundary without a phase change. At high temperature boundaries often lose the adsorption without a phase change. Low and high temperature properties often seem to belong to different phases, but careful examination often reveals continuity and thermodynamic consistency without a phase change.

In a polycrystalline specimen each boundary may have one or more phase transitions but these will occur at different temperatures for different boundaries. Observations on global properties of polycrystalline samples will smear out the phase transitions that do occur. Micrographic investigation for facetting changes seems to be the obvious way to survey all the many boundaries in a polycrystalline sample.



The most important conclusion of this paper is the clear identification between grain boundary phase change and facetting. It has been incorporated into our definition of phase change. Reports of phase changes on curved boundaries without the facetting evidence are not credible. The experimental test required by this definition is simple enough that we should now know when we have a phase transition.

Acknowledgment - I am grateful to Wm J. Boettinger for valuable criticism. The research on the wetting transitions was supported by NASA. The research on the melting transition was supported by AROD.

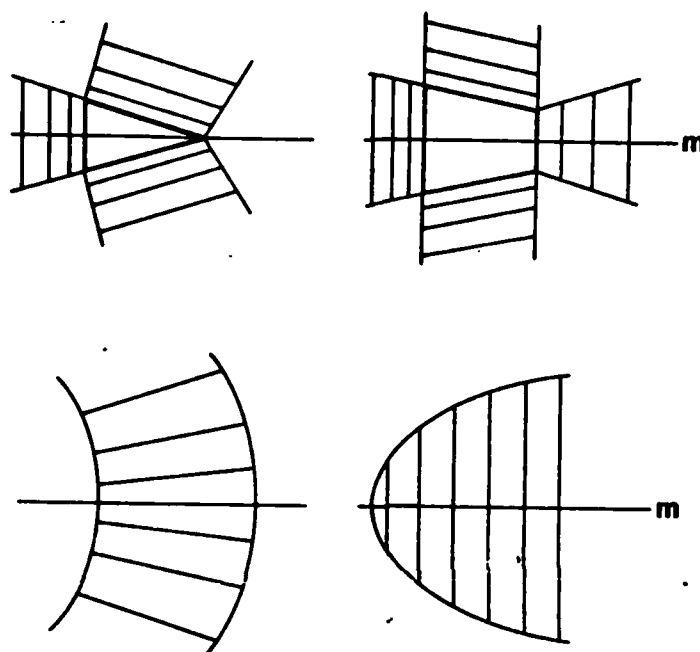


**Fig. 4** : Portions of an N diagram straddling a mirror plane. Multi-phase coexistence is marked by a tie triangle, a tie trapezoid and tie lines. Critical points between mirror related phases must lie on the mirror.

## References.

1. HART E. W., Scripta Met 2 (1968) 179.
2. HART E. W., "The Nature and Behavior of Grain Boundaries" H. Hu Ed. Plenum, NY(1972) 155.
3. GLEITER H., Z Met 61 (1970) 282, 978
4. KASEN M. B., Acta Met 20 (1972) 105, submitted to Acta Met (1982)
5. SIMPSON C. J. & AUST K. T., Surface Science 31 (1972) 479,497.
6. GLIKMAN Ye E., BRUVER R. E., KRASOV A. A., TRUBIN S. V., and KOTYSHEV V. F., Phys. Met. Metallog 37 (1974) #6-44; Fiz. Metal. Metalloved 37 (1974) 1174.
7. NICHOLS S. and LEWIS P. J., Scripta Met 11 (1977) 491.
8. GANGLOFF R. P. and WEI R. P., Scripta Met 8 (1974) 661; Met Trans 8A (1977) 1043.
9. CHAN N. H., Klier K., WEI R. P., Scripta Met 12 (1978) 1043.
10. GRABSKI M. W., KIRCHNER H. O. K., SHELL C. A., Z. Met. 61 (1970) 977.
11. GOUX C., Surface Science 31 (1972) 496.
12. SHELTON J. C., PATIL H. R., BLAKELY J. M., Surface Science 43 (1974) 493.
13. GUTTMANN M., Met. Trans. 8A (1977) 1383.
14. GIBBS J. W., Collected Works Yale Univ. Press (1948) V. 1, p.223.
15. CAHN J. W., "Thermodynamics of Solid and Fluid Surfaces" in Segregation to Interfaces, ASM Seminar Series (1978) 3.
16. KALONJI G., Symmetry Principles in the Physics of Crystalline Interfaces, Ph.D. Thesis, MIT (1982)
17. HERRMAN G, GLEITER H. and BAERO G, Acta Met 24 (1976) 353.
18. HERRING C., Phys Rev 82 (1951) 87.
19. HOFFMAN D. W. & CAHN J. W., Surface Science 31 (1972) 368.
20. PRINCE A., Alloy Phase Equilibria, Elsevier NY (1966)
21. DARKEN L. S. and GURRY R. W., Physical Chemistry of Metals, McGraw-Hill, NY (1953)
22. BAKER J. C. and CAHN J. W., Solidification ASM Seminar Series (1971) 23.
23. SCOTT R. L., J. Chem. Soc., Faraday Trans II, 73 (1977) 356.
24. PELTON A. D. and SCHMALZRIED H., Met Trans 4 (1973) 1395.
25. GOODHEW P.J., TAN T.Y. and BALLUFFI R.W., Acta Met 26 (1978) 557.
26. FRANK F. C., "The Geometrical Thermodynamics of Surfaces" in Metal Surfaces ASM Seminar Series (1962) 1.
27. CAHN J. W. and HOFFMAN D. W., Acta Met 22 (1974) 1205.
28. MULLINS W. W., "Solid Surface Morphologies Governed by Capillarity" in Metal Surfaces ASM Seminar Series (1962) 17.
29. MULLINS W. W., Phil Mag 6 (1961) 1313.
30. WAGNER W. R., TAN T. Y., and BALLUFFI R. W., Phil Mag 29 (1974) 895.
31. DEFAY R. and PRIGOGINE I., Surface Tension and Adsorption, Translated by EVERETT D.H., Wiley NY (1966) 77.
32. DEFAY R., Etude Thermodynamique de la Tension Superficielle, Paris (1934)
33. KALONJI G. and CAHN J. W., J. Physique, This Issue.
34. GRATIAS D., D. Sc. Thesis Universite Pierre et Marie Curie, Paris VI (1978)
35. POND R. C. and BOLLMANN W., Trans. Roy. Soc. 292 (1979) 1395
36. BUERGER M., Elementary Crystallography, MIT Press, Cambridge, MA (1978) Chapt. 10.
37. MULLINS W. W. and SEKERKA R. F., J. Phys. Chem. Solids 23 (1962) 801.
38. VOLD C. L. and GLICKSMAN M. E. in "The Nature and Behavior of Grain Boundaries" H. Hu Ed., Plenum, NY (1972) 171.
39. GLICKSMAN M. E. and VOLD C. L., Acta Met 17 (1969) 1.
40. KIKUCHI R. and CAHN J. W., Phys Rev B 21 (1980) 1893.
41. SMITH C. S., Trans Am Soc Met. 45 (1953) 533.
42. CAHN J. W., J. Chem. Phys. 66 (1977) 3667.
43. CAHN, J. W. and HILLIARD J. E., J. Chem. Phys. 28 (1958) 258.
44. GUIRALDENQ P. and LACOMBE P., Acta. Met. 13 (1965) 51.
45. DONALD A., Phil Mag 34 (1976) 1185.